

# Learning Soft Sparse Shapes for Efficient Time-Series Classification

Zhen Liu<sup>1,2</sup> Yicheng Luo<sup>1</sup> Boyuan Li<sup>1</sup> Emadeldeen Eldele<sup>2</sup> Min Wu<sup>†,2</sup> Qianli Ma<sup>†,1</sup>

## Abstract

Shapelets are discriminative subsequences (or shapes) with high interpretability in time series classification. Due to the time-intensive nature of shapelet discovery, existing shapelet-based methods mainly focus on selecting discriminative shapes while discarding others to achieve candidate subsequence sparsification. However, this approach may exclude beneficial shapes and overlook the varying contributions of shapelets to classification performance. To this end, we propose a **Soft** sparse **Shapes** (**SoftShape**) model for efficient time series classification. Our approach mainly introduces soft shape sparsification and soft shape learning blocks. The former transforms shapes into soft representations based on classification contribution scores, merging lower-scored ones into a single shape to retain and differentiate all subsequence information. The latter facilitates intra- and inter-shape temporal pattern learning, improving model efficiency by using sparsified soft shapes as inputs. Specifically, we employ a learnable router to activate a subset of class-specific expert networks for intra-shape pattern learning. Meanwhile, a shared expert network learns inter-shape patterns by converting sparsified shapes into sequences. Extensive experiments show that SoftShape outperforms state-of-the-art methods and produces interpretable results. Our code is available at <https://github.com/qianlima-lab/SoftShape>.

## 1. Introduction

Time series classification (TSC) is a critical task with various real-world applications, such as human activity recog-

<sup>1</sup> School of Computer Science and Engineering, South China University of Technology, Guangzhou, China <sup>2</sup>Institute for Infocomm Research, Agency for Science, Technology and Research, Singapore. Correspondence to: Qianli Ma <qianlima@scut.edu.cn>, Min Wu <wumin@i2r.a-star.edu.sg>.

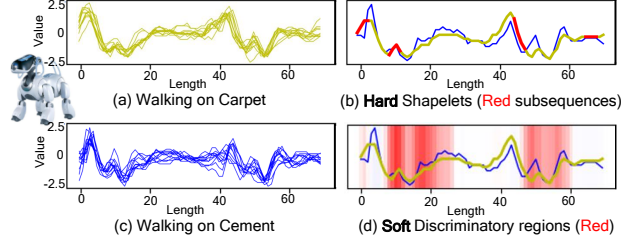


Figure 1: (a) Yellow and (c) Blue lines represent two time series class samples from the *SonyAIBORobotSurface1* UCR dataset. (b) Red subsequences denote shapelets for the “Walking on Carpet” class. (d) Red regions show discriminative parts of the “Walking on Carpet” class, with darker red indicating greater discriminative power.

nition (Lara & Labrador, 2012) and medical diagnostics (Wang et al., 2024). Unlike traditional data types, time series data consists of ordered numerical observations with temporal dependencies, which is often difficult for human intuition to understand. Recent studies (Mohammadi Foumani et al., 2024; Middlehurst et al., 2024; Jin et al., 2024; Ma et al., 2024) indicate that deep neural networks showed remarkable success in TSC, even without specialized knowledge. However, their black-box nature is a barrier to adopting effective models in critical applications such as healthcare, where insights about model decisions are important. Therefore, enhancing the interpretability of these models for TSC is a crucial ongoing issue.

Shapelets, which are discriminative subsequences that characterize target classes, offer a promising approach towards interpretable TSC models (Ye & Keogh, 2009). For instance, Figures 1(a) and 1(c) show time series classes of a robotic dog walking on carpet and cement (Vail & Veloso, 2004). The red subsequences shown in Figure 1(b) illustrate shapelets, as selected by Hou et al. (2016). However, identifying these shapelets is usually computationally intensive (Rakthanmanon & Keogh, 2013), as it requires evaluating subsequences across varying positions and lengths.

Existing methods (Grabocka et al., 2014; Li et al., 2020) address this issue via a shapelet transformation strategy for candidate subsequence sparsification. Specifically, they convert each subsequence into a feature that quantifies the distance between a time series sample and the subsequence (Ma

et al., 2020). Subsequently, this strategy was followed by many methods (Li et al., 2021; Le et al., 2024) to learn shapelet representations, thereby enhancing the model’s interpretability. While efficient, this approach discards many subsequences from the entire time series in a *hard* manner, those who could be beneficial for the classification tasks. In addition, this approach fails to account for the varying importance of shapelets to classification. As shown in Figure 1(b), this leads to poor capture of class patterns in the third and fourth subsequences due to minimal class differences, while omitting many informative regions.

Recent advances in time series patch tokenization (Nie et al., 2023; Bian et al., 2024), i.e., converting time series into subsequence-based tokens, and in the mixture of experts (MoE) architectures (Riquelme et al., 2021; Fedus et al., 2022) inspired a new direction. In computer vision, MoE routers dynamically assign input patches to specialized experts, which can improve both efficiency and class-specific feature learning (Chen et al., 2022; Chowdhury et al., 2023). By analogy, time series shapelets, which can exhibit intra-class similarity and inter-class distribution, can act as patch tokens, with MoE enabling adaptive focus on the most discriminative subsequences. Yet, existing shapelet-based methods overlooked such approach.

In this paper, we propose the **Soft sparse Shapes (SoftShape)** model for TSC, which replaces hard shapelet sparsification with soft shapelets. Specifically, we introduce a soft shape sparsification mechanism to reduce the number of learning shapes, thereby enhancing the efficiency of model training. To clarify our motivation, Figure 1(d) shows the classification results of InceptionTime (Ismail Fawaz et al., 2020) using multiple-instance learning (Early et al., 2024). Unlike the *hard* way depicted in Figure 1(b), our *soft* shapelet sparsification assigns weights to shapes based on their classification contribution scores, effectively preserving and differentiating all subsequence information from the time series. Furthermore, we enhance the discriminability of the learned soft shapes by combining: (1) Intra-shape patterns via MoE, where experts specialize in class-specific shapelet types; and (2) Inter-shape dependencies via a shared expert that models temporal relationships among sparsified shapes.

In summary, the major contributions are as follows:

- We propose SoftShape, a soft shapelet sparsification approach for TSC. This weighted aggregation of subsequences is based on contribution scores, avoiding information loss from hard filtering.
- We introduce a dual-pattern learning approach based on an MoE-driven intra-shape specialization and sequence-aware inter-shape modeling.
- We conduct extensive experiments on 128 UCR time se-

ries datasets, demonstrating the superior performance of our approach against state-of-the-art approaches while showcasing interpretable results.

## 2. Related Work

### 2.1. Deep Learning for Time-Series Classification

Recently, deep learning has garnered significant attention from scholars in TSC tasks due to its powerful feature extraction capabilities (Campos et al., 2023; Zhang et al., 2024). For example, Ismail Fawaz et al. (2019) and Mohammadi Foumani et al. (2024) have systematically reviewed deep learning approaches for TSC, focusing on different types of deep neural networks and deep learning paradigms, respectively. In addition, Middlehurst et al. (2024) and Ma et al. (2024) have conducted extensive experiments to evaluate recent TSC methods. Their findings demonstrate that deep learning models can be effectively applied to TSC tasks. Despite their strong performance, these deep learning-based TSC methods often struggle to improve the interpretability of classification results.

### 2.2. Time-Series Classification with Shapelets

Ye & Keogh (2009) first introduced shapelets, providing good interpretability for TSC results. Early methods (Mueen et al., 2011; Rakthanmanon & Keogh, 2013) selected the most discriminative subsequences as shapelets using an evaluation function, but the sparsification process was computationally intensive due to the numerous candidate subsequences. To tackle this problem, Hills et al. (2014) introduced the shapelet transform, converting all candidate subsequences into distance-based features for shapelet discovery. Recent studies (Qu et al., 2024; Le et al., 2024; Wen et al., 2025) have applied the shapelet transform strategy in deep learning for TSC, thereby improving model interoperability. However, these methods often handle candidate subsequences in a hard way, which easily leads to the loss of helpful temporal patterns from the time series sample.

More recently, Nie et al. (2023); Wu et al. (2025) showed that using patches of time series as input data enhances forecasting performance and reduces training time. Building on this, Luo & Wang (2024), Wang et al. (2024), and Wen et al. (2024) validated the effectiveness of patch techniques for TSC. Eldele et al. (2024) further demonstrated that using time series patches as CNN inputs outperformed Transformer-based methods. However, these methods typically use all patches as inputs, leading to computational inefficiency in TSC for long sequences.

### 2.3. Mixture-of-Experts in Time Series

Mixture of experts (MoE) typically consist of multiple sub-networks (experts) and a learnable router (Shazeer et al., 2017; Zhou et al., 2022). MoE has been utilized in time series forecasting for decades (Zeevi et al., 1996; Ni et al., 2024) and recently applied to improve the efficiency of foundational time series forecasting models (Shi et al., 2025; Liu et al., 2024a). Also, Huang et al. (2025) extended MoE to graph-based models for time series anomaly detection. Wen et al. (2025) introduced a gated router within MoE to integrate DNNs for learning time series representations, combining them with shapelet transform features to address the performance limitations of using shapelet transform alone in TSC. Unlike the above methods, we utilize the MoE router to activate class-specific experts for learning intra-shape local temporal patterns. Furthermore, we employ a shared expert to capture global temporal patterns across sparsified shapes from the same time series, thereby enhancing the discriminative power of shape embeddings.

## 3. Preliminaries

### 3.1. Problem Definition

In this study, we focus on using deep learning models for univariate time series classification. Let the time series dataset be represented as  $\mathcal{D} = \{(\mathcal{X}_n, \mathcal{Y}_n)\}_{n=1}^N$ , where  $N$  denotes the total number of time series samples. Each univariate time series  $\mathcal{X}_n = \{x_1, x_2, \dots, x_T\}$  is an ordered sequence of  $T$  real-valued observations. The corresponding label  $\mathcal{Y}_n \in \mathbb{R}^C$  is a one-hot encoded vector, where each value  $y_c \in \{0, 1\}$  indicates whether  $\mathcal{X}_n$  belongs to class  $c$ , with  $C$  representing the total number of classes. Given a deep learning model parameterized by  $\theta$ , the objective of the TSC task is to optimize the function  $f_\theta : \mathbb{R}^T \rightarrow \mathbb{R}^C$  such that it can accurately predict the label  $\mathcal{Y}_n$  corresponding to any input time series  $\mathcal{X}_n$ .

### 3.2. Time Series Shapelets

Given a time series  $\mathcal{X}_n$ , a subsequence of length  $m$ , where  $m < T$ , is denoted as  $\mathcal{S}_{n,p}^m = \{x_p, x_{p+1}, \dots, x_{p+m-1}\}$ . Here,  $p$  denotes the starting index of  $\mathcal{S}_{n,p}^m$ , where  $0 \leq p < T - m$ . All subsequences of length  $m$  from the time series  $\mathcal{X}_n$  can be extracted using a sliding window of size  $m$  with a fixed step size  $q$  (commonly  $q = 1$ ), traversing from  $t = 1$  to  $T$ . Thus, the set of all subsequences of length  $m$  from  $\mathcal{X}_n$  can be defined as  $\mathcal{S}_n^m = \{\mathcal{S}_{n,p}^m \mid 0 \leq p < T - m\}$ .

Owing to the length of the subsequences varying within the range  $2 \leq m \leq T - 1$ , the candidate set  $\mathcal{A}$  of all possible subsequences for the time series dataset  $\mathcal{D}$  is expressed as:

$$\mathcal{A} = \bigcup_{n=1}^N \bigcup_{m=2}^{T-1} \mathcal{S}_n^m = \{\mathcal{S}_{n,p}^m \mid 0 \leq p < T - m\}. \quad (1)$$

Shapelets are defined as a subset of discriminative subsequences within  $\mathcal{A}$  that maximally represent the class of each time series  $\mathcal{X}_n$  (Ye & Keogh, 2009). Given that every shape in  $\mathcal{A}$  could potentially serve as a shapelet, a brute-force search to evaluate all subsequences of each  $\mathcal{X}_n$  using an evaluation function becomes computationally prohibitive as the number of samples  $N$  and the sequence length  $T$  increase. Thus, the design of appropriate sparsification techniques for the set  $\mathcal{A}$  is crucial for enhancing the computational efficiency of shapelet-based TSC methods.

## 4. Methodology

### 4.1. Model Overview

The overall architecture of the SoftShape model is illustrated in Figure 2. SoftShape begins with a shape embedding layer that transforms the input time series into shape embeddings corresponding to multiple equal-length subsequences. These embeddings are normalized with a norm layer and then processed using soft shape sparsification (see Section 4.2). Specifically, an attention head assigns weight scores to each shape embedding based on its classification contribution. High-weight embeddings are scaled by their scores to form soft shapes, while low-weight embeddings are merged into a single shape for sparsification. The normalized sparsified shape embeddings are then input into the soft shape learning block to learn temporal patterns (see Section 4.3). Within this block, a MoE router activates a few class-specific experts to capture intra-shape temporal patterns (see Section 4.3.1). Meanwhile, these sparsified soft shapes are transformed into sequences, with a shared expert learning inter-shape temporal patterns (see Section 4.3.2). Finally, the sparsified soft shape embeddings, along with the intra-shape and inter-shape embeddings learned by the soft shape learning block, are combined in a residual way. After stacking  $L$  layers, the output is passed to a linear layer for classification training (see Section 4.4).

### 4.2. Soft Shape Sparsification

For each input time series  $\mathcal{X}_n$ , we use a 1D convolutional neural network (CNN) as the shape embedding layer to obtain  $M = \frac{T-m}{q} + 1$  ( $q < m$ ) overlapping subsequence embeddings, denoted  $\hat{\mathcal{S}}_n^m = \{\hat{\mathcal{S}}_{n,p}^m \mid 0 \leq p < T - m\}$ . Each shape embedding  $\hat{\mathcal{S}}_{n,p}^m$  is computed using the following convolution operation:

$$\hat{\mathcal{S}}_{n,p}^m = \left\{ \sum_{i=0}^{m-1} \mathbf{W}_i \mathcal{S}_{n,p}^m \mid p = 0, q, 2q, \dots, T - m \right\}, \quad (2)$$

where  $\mathbf{W}_i$  denotes the weights of the  $i$ -th filter within the kernel of the CNN, and  $\hat{\mathcal{S}}_{n,p}^m \in \mathbb{R}^d$ , with  $d$  representing the dimension of the shape embedding. Like patch-based methods (Nie et al., 2023; Eldele et al., 2024), we incorporate

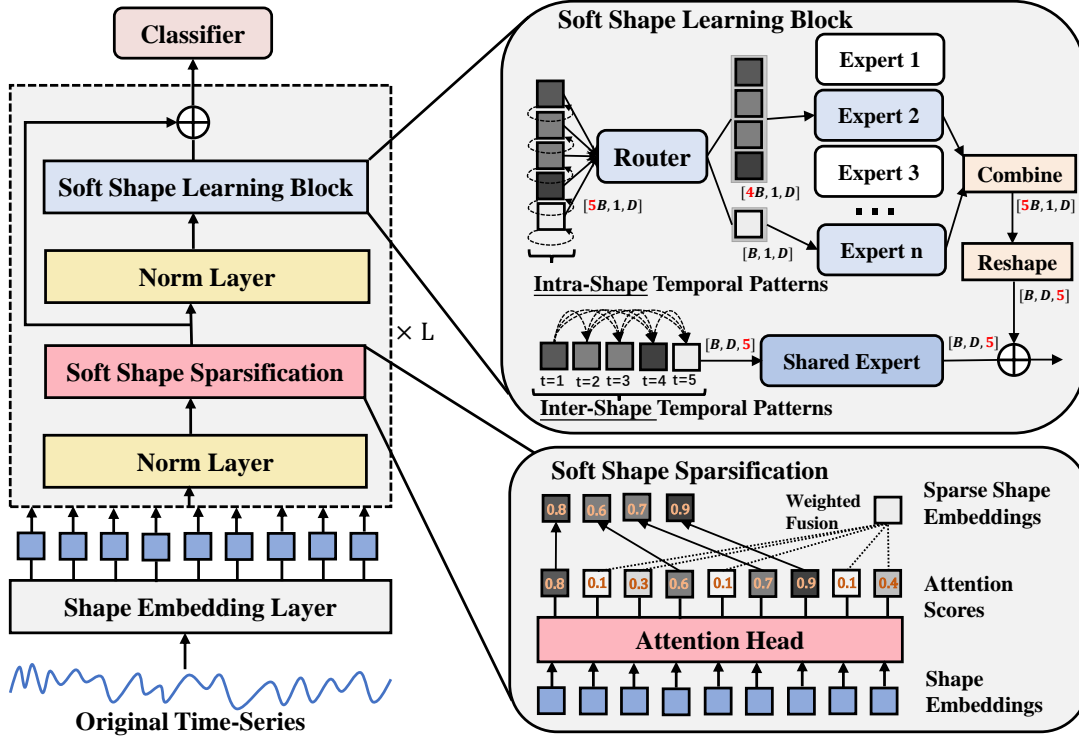


Figure 2: The general architecture of SoftShape model. SoftShape mainly involves: a) Soft Shape Sparsification converts shapes into soft forms and fuses those with lower scores into a single shape. b) Soft Shape Learning Block employs a MoE router to activate class-specific experts to learn intra-shape patterns and utilizes a shared expert to learn inter-shape patterns.

learnable positional embeddings into shape embeddings to capture temporal dependencies within the time series.

To identify the most discriminative shape embeddings in  $\hat{\mathcal{S}}_n^m$ , we employ a parameter-shared attention head across soft shape learning blocks at different depths. Unlike the self-attention mechanism in Transformers, we employ a gated attention mechanism (Ilse et al., 2018) that assumes independence among shape embeddings. This design facilitates label-guided identification of key shapes while maintaining linear computational complexity with respect to the number of shapes (Early et al., 2024). The attention head evaluates the contribution score of each  $\hat{\mathcal{S}}_{n,p}^m$  for classification training, defined as follows:

$$\alpha(\hat{\mathcal{S}}_{n,p}^m) = \sigma \left( \mathbf{W}_2 \tanh \left( \mathbf{W}_1 \hat{\mathcal{S}}_{n,p}^m + \mathbf{b}_1 \right) + \mathbf{b}_2 \right), \quad (3)$$

where  $\sigma(\cdot)$  is the sigmoid function outputting  $\alpha \in (0, 1)$ ,  $\tanh(\cdot)$  is the hyperbolic tangent function,  $\mathbf{W}_1 \in \mathbb{R}^{d_{\text{attn}} \times d}$  and  $\mathbf{W}_2 \in \mathbb{R}^{1 \times d_{\text{attn}}}$  are the weights of a linear layer, and  $\mathbf{b}_1 \in \mathbb{R}^{d_{\text{attn}}}$  and  $\mathbf{b}_2 \in \mathbb{R}$  are the bias terms.

The value of  $\alpha(\hat{\mathcal{S}}_{n,p}^m)$  closer to 1 indicates a greater contribution to enhancing classification performance. Hence, we

can perform soft shape sparsification using scores from the attention head based on their ranking. For each attention score of  $\hat{\mathcal{S}}_{n,p}^m$  ranked within the top  $\eta$  proportion among the total  $J = \frac{T-m}{q} + 1$  shapes embeddings in  $\hat{\mathcal{S}}_n^m$ , we convert them into soft shape embeddings as follows:

$$\tilde{\mathcal{S}}_{n,p}^m = \alpha(\hat{\mathcal{S}}_{n,p}^m) \hat{\mathcal{S}}_{n,p}^m. \quad (4)$$

For those with scores below the top  $\eta$  proportion, we fuse them into a single shape embedding as follows:

$$\tilde{\mathcal{S}}_{n,\text{fused}}^m = \sum_{p \in \mathcal{E}} \alpha(\hat{\mathcal{S}}_{n,p}^m) \hat{\mathcal{S}}_{n,p}^m, \quad (5)$$

where  $\mathcal{E}$  denotes the index of scores that are below the top  $\eta$  proportion. Finally, the soft shape embeddings are sorted according to their original order in  $\hat{\mathcal{S}}_n^m$ , with the fused embedding  $\tilde{\mathcal{S}}_{n,\text{fused}}^m$  appended at the end to form the sparsified soft shape embeddings  $\tilde{\mathcal{S}}_n^m$ .

Through this sparsification process, we transform the time series  $\mathcal{X}_n$  into sparsified soft shape embeddings  $\tilde{\mathcal{S}}_n^m$ . Compared to directly using all shape embeddings in  $\hat{\mathcal{S}}_n^m$  as input, the number of shape embeddings in  $\tilde{\mathcal{S}}_n^m$  is reduced, thereby decreasing the cost of the model's computation.



### 4.3. Soft Shape Learning Block

#### 4.3.1. INTRA-SHAPE LEARNING

Intuitively, shapelets from different classes show distinct temporal patterns, whereas those from the same class are more similar. Recently, [Chen et al. \(2022\)](#); [Chowdhury et al. \(2023\)](#) theoretically indicated that the MoE router can direct input embeddings with similar class patterns to the same expert while filtering out class-irrelevant features. This lets the router activate a few experts (sub-networks) for each shape embedding, learning class-specific features and reducing the number of trainable parameters compared to activating all experts simultaneously. Therefore, we introduce a module that employs the MoE router to activate class-specific experts for learning intra-shape temporal patterns, thereby enhancing the discriminative capability of each soft shape embedding. The function of the MoE router is defined as:

$$G(\tilde{\mathcal{S}}_{n,p}^m) = \text{TOP}_k(\text{softmax}(\mathbf{W}_t \tilde{\mathcal{S}}_{n,p}^m)), \quad (6)$$

$$\text{TOP}_k(v) = \begin{cases} v_i, & \text{if } v_i \text{ is in the top } k \text{ values of } v, \\ 0, & \text{otherwise.} \end{cases} \quad (7)$$

where  $\mathbf{W}_t \in \mathbb{R}^{\hat{C} \times d}$  are the learning weights of the router that convert the sparsified shape embedding  $\tilde{\mathcal{S}}_{n,p}^m$  into a vector of corresponding to the total number of experts  $\hat{C}$ . The  $\text{TOP}_k(v)$  is applied after the softmax function to prevent the values of  $G(\tilde{\mathcal{S}}_{n,p}^m)$  being zero almost everywhere during training ([Riquelme et al., 2021](#)), particularly when  $k = 1$ .

In the paper, each MoE expert employs a lightweight MLP network to learn class-specific patterns using each soft shape embedding as input. The  $e$ -th expert function is defined as:

$$h_e(\theta, \tilde{\mathcal{S}}_{n,p}^m) = \hat{G}_e(\tilde{\mathcal{S}}_{n,p}^m) \text{GeLU}(\mathbf{W}_e \tilde{\mathcal{S}}_{n,p}^m + \mathbf{b}_e), \quad (8)$$

$$\hat{G}_e(\tilde{\mathcal{S}}_{n,p}^m) = \frac{e^{G_e(\tilde{\mathcal{S}}_{n,p}^m)}}{\sum_{i \in \text{TOP}_k(v)} e^{G_i(\tilde{\mathcal{S}}_{n,p}^m)}}, \quad (9)$$

where  $\mathbf{W}_e$  and  $\mathbf{b}_e$  represent the weight and bias terms of the MLP network, and  $\text{GeLU}(\cdot)$  denotes the gaussian error linear unit activation function. The MoE experts' parameters are shared across soft shape learning blocks at different depths, ensuring the efficiency of parameter optimization.

However, the MoE router often tends to converge to a state where it assigns higher weights to a few favored experts. This imbalance can cause the favored experts to train faster and dominate the expert selection process, resulting in underutilization and potential underfitting of less frequently chosen experts. To address this issue, following ([Shazeer et al., 2017](#)), we employ two loss functions as follows:

$$\mathcal{L}_{\text{imp}}(\tilde{\mathcal{S}}_{n,p}^m) = \mathbf{W}_{\text{imp}} \text{CV} \left( \sum_{\tilde{\mathcal{S}}_{n,p}^m \in \tilde{\mathcal{S}}_n^m} G(\tilde{\mathcal{S}}_{n,p}^m) \right)^2, \quad (10)$$

where  $\mathbf{W}_{\text{imp}}$  is the learning weight parameters and  $\text{CV}(\cdot)$  denotes the coefficient of variation, thus ensuring all experts contribute equally.

$$\mathcal{L}_{\text{load}}(\tilde{\mathcal{S}}_{n,p}^m) = \mathbf{W}_{\text{load}} \text{CV}(\text{Load}(\tilde{\mathcal{S}}_{n,p}^m))^2, \quad (11)$$

where  $\mathbf{W}_{\text{load}}$  is the learning weight parameters for load balancing and  $\text{Load}(\tilde{\mathcal{S}}_{n,p}^m)$  is the number of soft shape embeddings assigned to each expert, thereby reducing the risk of underutilization. By jointly optimizing  $\mathcal{L}_{\text{imp}}$  and  $\mathcal{L}_{\text{load}}$  in the overall loss function, we can alleviate the likelihood of underfitting in some experts. In addition, following [Zoph et al. \(2022\)](#), we apply a residual connection between the input shape embedding  $\tilde{\mathcal{S}}_{n,p}^m$  and the output  $h_e(\theta, \tilde{\mathcal{S}}_{n,p}^m)$  to enhance training stability.

#### 4.3.2. INTER-SHAPE LEARNING

While the MoE router activates a few experts to learn class-specific temporal patterns within each soft shape, it treats the multiple shapes extracted from each time series sample independently, thereby overlooking the temporal dependencies among shapes. In general, learning intra-shape temporal patterns is beneficial for capturing local discriminative features, but it can be difficult to learn the global temporal patterns from the time series that are vital for classification. To this end, we introduce a shared expert to learn the temporal patterns among sparsified shapes within the time series.

The sparsified soft shape embeddings are first transformed into a sequence where each shape is treated as an individual unit. This transformation is defined as:

$$\mathcal{Q}_n^m = (\tilde{\mathcal{S}}_n^m)^T, \quad \text{where } \tilde{\mathcal{S}}_n^m \in \mathbb{R}^{B \times \text{Num} \times d}, \quad (12)$$

where  $\mathcal{Q}_n^m \in \mathbb{R}^{B \times d \times \text{Num}}$ , and  $B$  denotes the batch size,  $\text{Num} = J \times \eta + 1$  is the number of sparsified soft shapes of each time series, and  $d$  is the dimension of one soft shape embedding. Recent studies ([Middlehurst et al., 2024](#)) have shown that CNN-based models perform remarkably in TSC tasks. In this work, we employ a CNN-based Inception module ([Ismail Fawaz et al., 2020](#)) as the shared expert. The shared expert comprises three 1D convolutional layers with different kernel sizes, sliding along the third dimension of  $\mathcal{Q}_n^m$  from 0 to  $\text{Num}$ . This allows it to learn multi-resolution temporal patterns across soft shapes effectively. For raw input time series samples, the input dimension containing  $B$  univariate time series can be represented as  $(B, 1, T)$ , where  $T$  is the length of each time series. Traditional CNN-based methods ([Ismail Fawaz et al., 2020](#)) typically transform each point in the time series into  $d$ -dimensional embeddings, resulting in an input dimension of  $(B, d, T)$ . Unlike the above, we treat each shape as a sequence point and convert it into  $d$ -dimensional embeddings for training.

As shown in Equations (1) and (5), with a higher sparsity rate  $(1 - \eta)$ , the actual sequence length  $\text{Num}$  of  $\mathcal{Q}_n^m$  fed

into the shared expert is significantly smaller than  $T$ , thus reducing the model’s computational load. The shared expert ensures efficient learning of temporal patterns across sparsified soft shapes, better capturing global features of the time series for classification training.

#### 4.4. The Training of SoftShape

The SoftShape model stacks  $L$  layers of the soft shape learning block for classification training. Each layer’s output is processed using a  $\text{GeLU}(\cdot)$  activation function. The final layer outputs three types of embeddings: the sparsified soft shape embeddings, the intra-shape embeddings, which are combined through a residual way denoted as  $O_n^m$ . To accurately represent the learned attention scores for each shape embedding associated with the target class, we employ conjunctive pooling (Early et al., 2024) for training:

$$\hat{\mathcal{Y}}_n = \frac{1}{Num} \sum_{i=0}^{Num} \alpha(O_n^m) \phi(O_{n,i}^m), \quad (13)$$

where  $\phi$  denotes a linear layer as the classifier. For all time series samples, we use the cross-entropy loss for classification training, defined as:

$$\mathcal{L}_{ce}(\mathcal{X}, \mathcal{Y}) = -\frac{1}{B} \sum_{i=1}^B \sum_{j=1}^C 1\{y_i = j\} \log(\hat{\mathcal{Y}}_i^j), \quad (14)$$

where  $\hat{\mathcal{Y}}_i^j$  is the predicted class probability at the  $j$ -th class for the sample  $\mathcal{X}_i$ . Therefore, the overall training objective for SoftShape is given by:

$$\mathcal{L}_{total} = \mathcal{L}_{ce} + \lambda(\mathcal{L}_{imp} + \mathcal{L}_{load}), \quad (15)$$

where  $\lambda$  is a hyperparameter to adjust the training loss ratio. Additionally, the pseudo-code for SoftShape can be found in Algorithm 1 located in the Appendix.

## 5. Experiments

To evaluate the performance of various methods for TSC, we conduct experiments using the UCR time series archive (Dau et al., 2019), a widely recognized benchmark in TSC (Ismail Fawaz et al., 2019). Many datasets in the UCR archive contain a significantly higher number of test samples compared to the training samples. Also, the original UCR time series datasets lack a specific validation set, increasing the risk of overfitting in deep learning methods. Following (Dau et al., 2019; Ma et al., 2024), we merge the original training and test sets of each UCR dataset. These merged datasets are then divided into train-validation-test sets at a ratio of 60%-20%-20%. This paper compares SoftShape against 19 baseline methods, categorized as follows:

- Deep Learning Methods (DL):

- *CNN-based (DL-CNN)*: FCN (Wang et al., 2017), T-Loss (Franceschi et al., 2019), SelfTime (Fan et al., 2020), TS-TCC (Eldele et al., 2021), TS2Vec (Yue et al., 2022), TimesNet (Wu et al., 2023b), InceptionTime (Ismail Fawaz et al., 2020), LightTS (Campos et al., 2023), ShapeConv (Qu et al., 2024), ModernTCN (Luo & Wang, 2024), and TSLANet (Eldele et al., 2024).
- *Transformer-based (DL-Trans)*: TST (Zerveas et al., 2021), PatchTST (Nie et al., 2023), Shapeformer (Le et al., 2024), and Medformer (Wang et al., 2024).
- *Foundation models (DL-FM)*: GPT4TS (Zhou et al., 2023) and UniTS (Gao et al., 2024).

- Non-Deep Learning Methods (Non-DL): RDST (Guillaume et al., 2022) and MultiRocket-Hydra (MR-H) (Dempster et al., 2023).

For information on datasets, baselines, and implementation details, please refer to Appendix A.

### 5.1. Main Results

Table 1: Test classification accuracy comparisons on 128 UCR time series datasets. The best results are in **bold**, and the second best results are underlined.

	Methods	Avg. Acc	Avg. Rank	Win	P-value
DL-CNN	FCN	0.8296	9.53	13	1.43E-12
	T-Loss	0.8325	11.12	9	2.95E-14
	SelfTime	0.8017	13.80	0	4.53E-25
	TS-TCC	0.7807	13.96	0	1.60E-15
	TS2Vec	0.8691	8.43	9	1.69E-15
	TimesNet	0.8367	10.13	7	4.22E-15
	InceptionTime	0.9181	4.05	29	7.39E-06
	ShapeConv	0.7688	13.91	5	3.58E-24
	ModernTCN	0.7938	11.37	9	1.78E-18
	TSLANet	<u>0.9205</u>	<u>3.68</u>	<u>31</u>	1.06E-03
DL-Trans	TST	0.7755	13.54	1	2.00E-19
	PatchTST	0.8265	9.56	12	1.27E-15
	Medformer	0.8541	9.26	7	7.15E-16
DL-FM	GPT4TS	0.8593	9.34	6	7.89E-16
	UniTS	0.8502	9.66	5	1.41E-13
Non-DL	RDST	0.8897	6.41	23	7.54E-10
	MR-H	0.8972	5.51	29	3.80E-07
	<b>SoftShape (Ours)</b>	<b>0.9334</b>	<b>2.72</b>	<b>53</b>	-

The classification accuracies on the test sets of the 128 UCR datasets are presented in Table 1, with detailed results provided in Appendix B.1. The average ranking (Avg. Rank) reflects the method’s relative position based on test accuracy, where lower values signify higher accuracy. Win indicates the number of datasets where the baseline achieves the highest test accuracy. The  $P$ -value from the Wilcoxon signed-rank test (Demšar, 2006) assesses the significance of

differences in test accuracy between pairwise methods. A  $P$ -value  $< 0.05$  suggests SoftShape outperforms the baseline.

Due to the high computational cost of LightTS (Campos et al., 2023) and Shapeformer (Le et al., 2024), their results are reported only on 18 selected UCR time series datasets in Table 10 of Appendix B.1. Detailed reasons for 18 UCR dataset selection are in Appendix B.3. The experimental results in Table 1 and Table 10 highlight SoftShape’s superior classification performance, demonstrating its effectiveness in TSC. Also, the P-value results confirm the statistical significance of SoftShape’s performance compared to baselines, highlighting its capacity to capture the discriminative patterns of time series data. The critical diagram (Figure 6) in the Appendix further supports the statistical significance of SoftShape’s performance improvement.

## 5.2. Ablation Study

Table 2: Test accuracy of ablation study on 128 UCR datasets. The best results are in **bold**, and the second best results are underlined.

Methods	Avg. Acc	Avg. Rank	Win	P-value
w/o Soft Sparse	0.9123	3.04	29	4.69E-06
w/o Intra	<u>0.9245</u>	<u>2.75</u>	<u>31</u>	5.39E-04
w/o Inter	<u>0.9022</u>	<u>3.74</u>	<u>19</u>	1.81E-09
w/o Intra & Inter	0.8696	5.02	11	4.35E-16
with Linear Shape	0.9164	3.23	22	1.80E-09
<b>SoftShape (Ours)</b>	<b>0.9334</b>	<b>2.04</b>	<b>60</b>	-

The ablation studies include: 1) **w/o Soft Sparse** removes the soft sparse process, using only the selected top  $\eta$  shape embeddings for training; 2) **w/o Intra** eliminates the intra-shape learning process via the class-specific experts; 3) **w/o Inter** removes the inter-shape learning process via the shared expert; 4) **w/o Intra & Inter** excludes both the intra-shape learning and inter-shape learning processes; 5) **with Linear Shape** employs a linear layer commonly used in (Nie et al., 2023; Wang et al., 2024) to replace the 1D CNN in Equation (2) as the shape embedding layer.

Table 2 presents the statistical ablation results, with detailed results provided in Appendix B.2. **w/o Soft Sparse** reduces accuracy and lowers the Avg. Rank, indicating the importance of this process in capturing the most helpful shape embeddings for classification. Similarly, **w/o Intra** highlights the significant role of the intra-shape module in SoftShape. Moreover, **w/o Inter** leads to a large drop in performance, underscoring the critical contribution of inter-shape relationships in learning global patterns of time series. When both the intra- and inter-shape learning processes are excluded (**w/o Intra & Inter**), performance further degrades, demonstrating that these two processes are foundational to SoftShape’s effectiveness. Finally, **with Linear Shape** con-

firms the superiority of the CNN architecture for learning shape embeddings. These results confirm the importance of each component in the SoftShape model.

## 5.3. Shape Sparsification and Learning Analysis

Table 3: Test accuracy of different sparse ratios on 18 UCR datasets. The best results are in **bold**, and the second best results are underlined.

Sparse Ratio	Avg. Acc	Avg. Rank	Win	P-value
0%	<u>0.9461</u>	<u>2.44</u>	4	-
10%	<b>0.9469</b>	<b>2.39</b>	<b>7</b>	2.97E-01
30%	0.9448	2.78	5	2.66E-01
50%	0.9453	2.61	<u>6</u>	3.46E-01
70%	0.9323	3.89	5	9.37E-03
90%	0.9261	4.50	2	4.02E-04

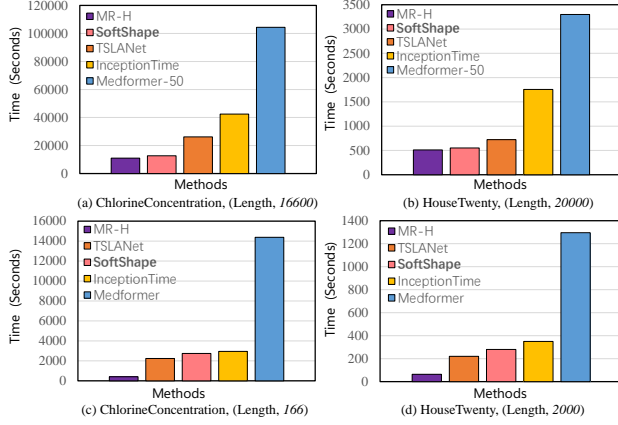
Evaluating all 128 UCR time series datasets takes considerable time, so we selected 18 datasets from the UCR time series archive for analysis and subsequent experiments. Table 3 presents the test results when combining shape embeddings with weighted fusion at varying sparse ratio  $(1 - \eta)$  proportions during sparsification, with detailed results provided in Appendix B.3. When  $(1 - \eta) \leq 50\%$ , test accuracy showed no significant decline compared to the non-sparsified case (0%), with all p-values  $> 0.05$ . Conversely, when  $(1 - \eta) > 50\%$ , particularly at 90%, performance declined significantly compared to 0%, indicating that excessive sparsification can remove some shape embeddings beneficial for capturing inter-shape global temporal patterns. Furthermore, the performance degradation under high sparsity ratios suggests that hard shapelet-based methods discard numerous informative subsequences, which may result in the loss of critical patterns useful for classification. As performance at 50% is statistically comparable to 0%, we set  $\eta$  to 50% in the main experiments to optimize the computational efficiency of the soft shape learning block.

Table 4 illustrates the effect of the number of activated experts ( $k$ ) selected by the MoE router during intra-shape learning, with detailed results provided in Appendix B.3. The results show that when  $k = 3$  or  $k = 4$ , the average rank is worse than when  $k = 1$  or  $k = 2$ . This suggests that activating a greater number of class-specific experts for each soft shape increases computational cost while diminishing the class discriminability of the intra-shape embeddings.

Also, we select one non-deep learning method (MR-H) and three deep learning baselines for runtime analysis. MR-H uses randomly initialized convolutional kernels for feature extraction, with training times measured on a CPU. The deep learning methods are evaluated on a GPU. Inception-Time is an advanced deep learning method described in

Table 4: Test accuracy comparison of the number of activated experts on 18 UCR datasets. The best result is in **bold**.

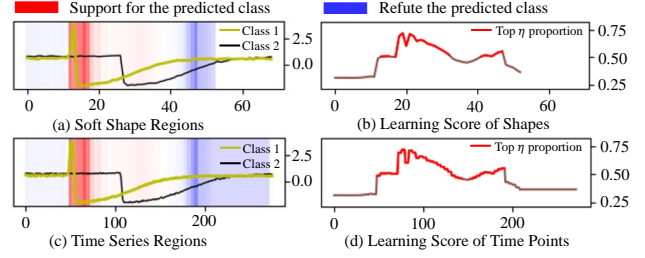
Activated Experts	$k=1$	$k=2$	$k=3$	$k=4$
Avg. Rank	<b>1.89</b>	1.94	2.78	2.39


 Figure 3: Running time analysis on the *ChlorineConcentration* and *HouseTwenty* datasets.

(Middlehurst et al., 2024). TSLANet and Medformer are recent patch-based models utilizing CNNs and Transformers, respectively. To evaluate SoftShape’s sparsification efficiency, we select two datasets: *ChlorineConcentration* (4,307 samples, length 166) and *HouseTwenty* (159 samples, length 2,000). In Figures 3(a) and 3(b), sequence lengths are extended to 16,600 and 20,000 by sample concatenation to simulate long-sequence scenarios. Given Medformer’s high computational cost for long sequences, we report only its runtime at 50 epochs (out of a maximum of 500), denoted as Medformer-50. As shown in Figures 3(a) and 3(b), SoftShape outperforms all deep learning baselines and is slightly slower than MR-H. Specifically, Medformer’s self-attention leads to higher training time with long sequences, while SoftShape’s linear-complexity gated attention ensures greater efficiency. In short-sequence [Figure 3(c)] and small-sample [Figure 3(d)] scenarios, SoftShape exhibits slightly higher runtime than TSLANet and substantially higher than MR-H. In these settings, sparsification offers limited efficiency gains, as the number of sparsified shapes does not decrease significantly compared to a greater number of training samples with long sequences. Additionally, Table 14 in Appendix B.3 presents the inference times and parameter counts for the settings in Figures 3(c) and 3(d).

#### 5.4. Visualization Analysis

To evaluate SoftShape’s effectiveness and interpretability, we use Multiple Instance Learning (MIL) (Early et al., 2024) for visualization. MIL identifies key time points in time se-


 Figure 4: The MIL visualization on the *Trace* dataset.

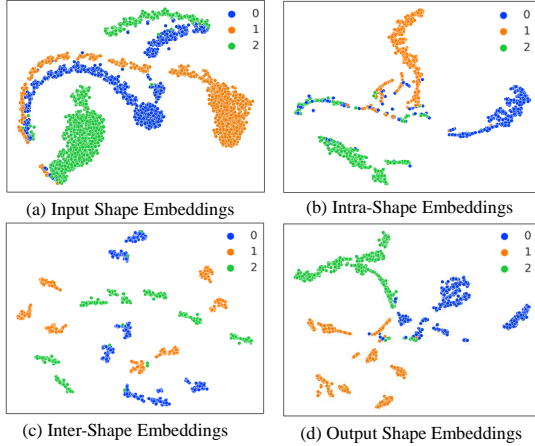
ries that improve classification performance. This study applies MIL to highlight significant shapes. Figure 4 shows the discriminative regions and attention scores learned by SoftShape on *Class 1* of the *Trace* dataset. Deeper red indicates beneficial regions for classification, while deeper blue shows less relevant ones. Figures 4(a) and 4(b) treat each shape (length  $m = 64$ ) as one sequence point, while Figures 4(c) and 4(d) map these results to the entire time series. SoftShape assigns higher attention scores to subsequences with significant differences between *Class 1* and *Class 2*, while sparsifying less discriminative regions. These findings indicate that SoftShape learns highly discriminative shapes as shapelets, enhancing interpretability through attention scores. Further MIL visualisations on the *Lightning2* dataset in the Appendix of Figure 7 support this finding.

The t-distributed Stochastic Neighbor Embedding (t-SNE) (Van der Maaten & Hinton, 2008) is used to visualize shape embeddings learned by SoftShape. Figure 5(a) shows input shape embeddings from 1D CNN (Eq. (2)) on the *CBF* dataset. Figures 5(b) and 5(c) present sparsified intra-shape and inter-shape embeddings from the soft shape learning block, while Figure 5(d) displays final output sparsified shape embeddings for classification. Compared to Figure 5(a), the intra-shape embeddings [Figure 5(b)] learned by activating class-specific experts form clusters for samples of the same class but still mix some samples from different classes. The inter-shape embeddings [Figure 5(c)] learned by a shared expert effectively separate different classes while dispersing same-class samples into multiple clusters. Combining intra- and inter-shape embeddings, Figure 5(d) balances class distinction and clusters samples of the same class closely together. These results indicate that SoftShape leverages intra- and inter-shape patterns to improve shape embedding discriminability. Further t-SNE visualization on the *TwoPatterns*, *Fiftywords*, and *ECG200* datasets with different classification difficulty can be seen in the Appendix of Figures 8, 9, and 10, respectively.

#### 5.5. Hyperparameter Analysis

Table 5 presents the classification results of SoftShape for various sliding fixed step sizes  $q$ . We observed a lower Avg.



Figure 5: The t-SNE visualization on the *CBF* dataset.Table 5: Test accuracy comparison of different sliding window sizes on 18 UCR datasets. The best result is in **bold**.

Sliding Step Size	$q=1$	$q=2$	$q=3$	$q=4$	$q=m$
Avg. Rank	3.83	2.78	2.44	<b>1.78</b>	2.94

Table 6: Test accuracy comparison of model depth on 18 UCR datasets. The best result is in **bold**.

Depth	$L=1$	$L=2$	$L=3$	$L=4$	$L=5$	$L=6$
Avg. Rank	3.72	<b>2.61</b>	3.06	3.33	3.44	3.06

Rank when  $q = 1$  or  $q = m$  (non-overlapping). With  $q = 1$ , the maximum subsequences result in redundancy and irrelevant information. Conversely,  $q = m$  generates the fewest subsequences, possibly missing important discriminative subsequences. Table 6 examines the influence of model depth  $L$ , revealing that SoftShape achieves the lowest Avg. Rank at  $L = 2$ , demonstrating shape embeddings capture discriminative features effectively, even at low depths. Detailed results of Tables 5 and 6 provided in Appendix B.4. Also, Tables 18, 19, 20, and 21 in Appendix B.4 present statistical test results on the impact of the maximum number of class-specific experts, class-specific expert networks, shared expert networks, and the hyperparameter  $\lambda$ .

To evaluate the impact of the hyperparameter shape length  $m$  on classification performance, we conducted three experiments: (1) Val-Select: Choose a fixed  $m$  for one SoftShape model using the validation set. (2) Fixed-8: Set  $m = 8$  for one SoftShape model. (3) Multi-Seq: Use fixed lengths (8, 16, 32) in parallel three SoftShape models, with cross-scale residual fusion (Liu et al., 2023) for classification. As shown in Table 7 (detailed results in Appendix B.4), there was no significant difference in performance between

Val-Select and Multi-Seq ( $p\text{-value} < 0.05$ ). The Val-Select model also has fewer parameters and a lower runtime. In addition, Tables 22 and 23 in Appendix B.5 present analyses of SoftShape’s time series forecasting performance.

Table 7: Test accuracy comparison of shape length  $m$  on 18 UCR datasets. The best result is in **bold**.

Methods	Val-Select	Fixed-8	Multi-Seq
Avg. Rank	1.72	2.28	<b>1.44</b>
P-value	2.88E-01	4.68E-02	-

## 6. Conclusion

In this paper, we propose a soft sparse shapes model for efficient TSC. Specifically, we introduce a soft shape sparsification mechanism that merges low-discriminative subsequences into a single shape based on learned attention scores, reducing the number of shapes for shape learning. Moreover, we propose a soft shape learning block for learning intra-shape and inter-shape temporal patterns, enhancing shape embedding discriminability. Extensive experiments demonstrate that SoftShape achieves state-of-the-art classification performance while providing interpretable results. However, this study does not consider the modelling of relationships among multiple variables of the time series. In future, we will investigate deep learning methods for multivariate TSC.

## Acknowledgements

We thank the anonymous reviewers for their helpful feedbacks. We thank Professor Eamonn Keogh and all the people who have contributed to the UCR time series classification archive. Zhen Liu and Yicheng Luo equally contributed to this work. The work described in this paper was partially funded by the National Natural Science Foundation of China (Grant No. 62272173), the Natural Science Foundation of Guangdong Province (Grant Nos. 2024A1515010089, 2022A1515010179), the Science and Technology Planning Project of Guangdong Province (Grant No. 2023A0505050106), the National Key R&D Program of China (Grant No. 2023YFA1011601), and the China Scholarship Council program (Grant No. 202406150081).

## Impact Statement

Our proposed work SoftShape aims to advance the field of Machine Learning by providing a more efficient and interpretable model for time series classification across various applications. There are many potential societal consequences of our work, none which we feel must be specifically highlighted here.

## References

- Bian, Y., Ju, X., Li, J., Xu, Z., Cheng, D., and Xu, Q. Multi-patch prediction: Adapting language models for time series representation learning. In *Forty-first International Conference on Machine Learning*, 2024.
- Campos, D., Zhang, M., Yang, B., Kieu, T., Guo, C., and Jensen, C. S. Lightts: Lightweight time series classification with adaptive ensemble distillation. *Proceedings of the ACM on Management of Data*, 1(2):1–27, 2023.
- Chen, Z., Deng, Y., Wu, Y., Gu, Q., and Li, Y. Towards understanding the mixture-of-experts layer in deep learning. *Advances in neural information processing systems*, 35: 23049–23062, 2022.
- Chowdhury, M. N. R., Zhang, S., Wang, M., Liu, S., and Chen, P.-Y. Patch-level routing in mixture-of-experts is provably sample-efficient for convolutional neural networks. In *International Conference on Machine Learning*, pp. 6074–6114. PMLR, 2023.
- Dau, H. A., Bagnall, A., Kamgar, K., Yeh, C.-C. M., Zhu, Y., Gharghabi, S., Ratanamahatana, C. A., and Keogh, E. The ucr time series archive. *IEEE/CAA Journal of Automatica Sinica*, 6(6):1293–1305, 2019.
- Dempster, A., Schmidt, D. F., and Webb, G. I. Hydra: Competing convolutional kernels for fast and accurate time series classification. *Data Mining and Knowledge Discovery*, 37(5):1779–1805, 2023.
- Demšar, J. Statistical comparisons of classifiers over multiple data sets. *The Journal of Machine learning research*, 7:1–30, 2006.
- Early, J., Cheung, G., Cutajar, K., Xie, H., Kandola, J., and Twomey, N. Inherently interpretable time series classification via multiple instance learning. In *The Twelfth International Conference on Learning Representations*, 2024.
- Eldele, E., Ragab, M., Chen, Z., Wu, M., Kwoh, C. K., Li, X., and Guan, C. Time-series representation learning via temporal and contextual contrasting. In *Proceedings of the Thirtieth International Joint Conference on Artificial Intelligence*, 2021.
- Eldele, E., Ragab, M., Chen, Z., Wu, M., and Li, X. Tslanet: Rethinking transformers for time series representation learning. In *Forty-first International Conference on Machine Learning*, 2024.
- Fan, H., Zhang, F., and Gao, Y. Self-supervised time series representation learning by inter-intra relational reasoning. *arXiv preprint arXiv:2011.13548*, 2020.
- Fedus, W., Zoph, B., and Shazeer, N. Switch transformers: Scaling to trillion parameter models with simple and efficient sparsity. *Journal of Machine Learning Research*, 23(120):1–39, 2022.
- Franceschi, J.-Y., Dieuleveut, A., and Jaggi, M. Unsupervised scalable representation learning for multivariate time series. *Advances in neural information processing systems*, 32, 2019.
- Gao, S., Koker, T., Queen, O., Hartvigsen, T., Tsiligkaridis, T., and Zitnik, M. Units: A unified multi-task time series model. *Advances in Neural Information Processing Systems*, 37:140589–140631, 2024.
- Grabocka, J., Schilling, N., Wistuba, M., and Schmidt-Thieme, L. Learning time-series shapelets. In *Proceedings of the 20th ACM SIGKDD international conference on Knowledge discovery and data mining*, pp. 392–401, 2014.
- Guillaume, A., Vrain, C., and Elloumi, W. Random dilated shapelet transform: A new approach for time series shapelets. In *International Conference on Pattern Recognition and Artificial Intelligence*, pp. 653–664. Springer, 2022.
- Hills, J., Lines, J., Baranauskas, E., Mapp, J., and Bagnall, A. Classification of time series by shapelet transformation. *Data mining and knowledge discovery*, 28:851–881, 2014.
- Hou, L., Kwok, J., and Zurada, J. Efficient learning of time-series shapelets. In *Proceedings of the AAAI Conference on Artificial Intelligence*, volume 30, 2016.
- Huang, X., Chen, W., Hu, B., and Mao, Z. Graph mixture of experts and memory-augmented routers for multivariate time series anomaly detection. In *Proceedings of the AAAI Conference on Artificial Intelligence*, volume 39, pp. 17476–17484, 2025.
- Ilse, M., Tomczak, J., and Welling, M. Attention-based deep multiple instance learning. In *International conference on machine learning*, pp. 2127–2136. PMLR, 2018.
- Ismail Fawaz, H., Forestier, G., Weber, J., Idoumghar, L., and Muller, P.-A. Deep learning for time series classification: a review. *Data mining and knowledge discovery*, 33(4):917–963, 2019.
- Ismail Fawaz, H., Lucas, B., Forestier, G., Pelletier, C., Schmidt, D. F., Weber, J., Webb, G. I., Idoumghar, L., Muller, P.-A., and Petitjean, F. Inceptiontime: Finding alexnet for time series classification. *Data Mining and Knowledge Discovery*, 34(6):1936–1962, 2020.

- Jin, M., Koh, H. Y., Wen, Q., Zambon, D., Alippi, C., Webb, G. I., King, I., and Pan, S. A survey on graph neural networks for time series: Forecasting, classification, imputation, and anomaly detection. *IEEE Transactions on Pattern Analysis and Machine Intelligence*, 2024.
- Langley, P. Crafting papers on machine learning. In Langley, P. (ed.), *Proceedings of the 17th International Conference on Machine Learning (ICML 2000)*, pp. 1207–1216, Stanford, CA, 2000. Morgan Kaufmann.
- Lara, O. D. and Labrador, M. A. A survey on human activity recognition using wearable sensors. *IEEE communications surveys & tutorials*, 15(3):1192–1209, 2012.
- Le, X.-M., Luo, L., Aickelin, U., and Tran, M.-T. Shapeformer: Shapelet transformer for multivariate time series classification. In *Proceedings of the 30th ACM SIGKDD Conference on Knowledge Discovery and Data Mining*, pp. 1484–1494, 2024.
- Li, G., Choi, B., Xu, J., Bhowmick, S. S., Chun, K.-P., and Wong, G. L.-H. Efficient shapelet discovery for time series classification. *IEEE transactions on knowledge and data engineering*, 34(3):1149–1163, 2020.
- Li, G., Choi, B., Xu, J., Bhowmick, S. S., Chun, K.-P., and Wong, G. L.-H. Shapenet: A shapelet-neural network approach for multivariate time series classification. In *Proceedings of the AAAI conference on artificial intelligence*, volume 35, pp. 8375–8383, 2021.
- Liu, X., Liu, J., Woo, G., Aksu, T., Liang, Y., Zimmermann, R., Liu, C., Savarese, S., Xiong, C., and Sahoo, D. Moirai-moe: Empowering time series foundation models with sparse mixture of experts. *arXiv preprint arXiv:2410.10469*, 2024a.
- Liu, Y., Hu, T., Zhang, H., Wu, H., Wang, S., Ma, L., and Long, M. itransformer: Inverted transformers are effective for time series forecasting. In *The Twelfth International Conference on Learning Representations*, 2024b.
- Liu, Z., Chen, D., Pei, W., Ma, Q., et al. Scale-teaching: Robust multi-scale training for time series classification with noisy labels. *Advances in Neural Information Processing Systems*, 36:33726–33757, 2023.
- Luo, D. and Wang, X. Modernrtn: A modern pure convolution structure for general time series analysis. In *The Twelfth International Conference on Learning Representations*, 2024.
- Ma, Q., Zhuang, W., Li, S., Huang, D., and Cottrell, G. Adversarial dynamic shapelet networks. In *Proceedings of the AAAI conference on artificial intelligence*, volume 34, pp. 5069–5076, 2020.
- Ma, Q., Liu, Z., Zheng, Z., Huang, Z., Zhu, S., Yu, Z., and Kwok, J. T. A survey on time-series pre-trained models. *IEEE Transactions on Knowledge and Data Engineering*, 36(12):7536–7555, 2024.
- Middlehurst, M., Large, J., Flynn, M., Lines, J., Bostrom, A., and Bagnall, A. Hive-cote 2.0: a new meta ensemble for time series classification. *Machine Learning*, 110(11): 3211–3243, 2021.
- Middlehurst, M., Schäfer, P., and Bagnall, A. Bake off redux: a review and experimental evaluation of recent time series classification algorithms. *Data Mining and Knowledge Discovery*, pp. 1–74, 2024.
- Mohammadi Foumani, N., Miller, L., Tan, C. W., Webb, G. I., Forestier, G., and Salehi, M. Deep learning for time series classification and extrinsic regression: A current survey. *ACM Computing Surveys*, 56(9):1–45, 2024.
- Mueen, A., Keogh, E., and Young, N. Logical-shapelets: an expressive primitive for time series classification. In *Proceedings of the 17th ACM SIGKDD international conference on Knowledge discovery and data mining*, pp. 1154–1162, 2011.
- Ni, R., Lin, Z., Wang, S., and Fanti, G. Mixture-of-linear-experts for long-term time series forecasting. In *International Conference on Artificial Intelligence and Statistics*, pp. 4672–4680. PMLR, 2024.
- Nie, Y., Nguyen, N. H., Sinthong, P., and Kalagnanam, J. A time series is worth 64 words: Long-term forecasting with transformers. In *The Eleventh International Conference on Learning Representations*, 2023.
- Qu, E., Wang, Y., Luo, X., He, W., Ren, K., and Li, D. Cnn kernels can be the best shapelets. In *The Twelfth International Conference on Learning Representations*, 2024.
- Rakthanmanon, T. and Keogh, E. Fast shapelets: A scalable algorithm for discovering time series shapelets. In *proceedings of the 2013 SIAM International Conference on Data Mining*, pp. 668–676. SIAM, 2013.
- Riquelme, C., Puigcerver, J., Mustafa, B., Neumann, M., Jenatton, R., Susano Pinto, A., Keyser, D., and Houlisby, N. Scaling vision with sparse mixture of experts. *Advances in Neural Information Processing Systems*, 34: 8583–8595, 2021.
- Shazeer, N., Mirhoseini, A., Maziarz, K., Davis, A., Le, Q., Hinton, G., and Dean, J. Outrageously large neural networks: The sparsely-gated mixture-of-experts layer. In *International Conference on Learning Representations*, 2017.

- Shi, X., Wang, S., Nie, Y., Li, D., Ye, Z., Wen, Q., and Jin, M. Time-moe: Billion-scale time series foundation models with mixture of experts. In *The Twelfth International Conference on Learning Representations*, 2025.
- Vail, D. and Veloso, M. Learning from accelerometer data on a legged robot. *IFAC Proceedings Volumes*, 37(8): 822–827, 2004.
- Van der Maaten, L. and Hinton, G. Visualizing data using t-sne. *Journal of machine learning research*, 9(11), 2008.
- Wang, Y., Huang, N., Li, T., Yan, Y., and Zhang, X. Med-former: A multi-granularity patching transformer for medical time-series classification. In *The Thirty-eighth Annual Conference on Neural Information Processing Systems*, 2024.
- Wang, Z., Yan, W., and Oates, T. Time series classification from scratch with deep neural networks: A strong baseline. In *2017 International joint conference on neural networks (IJCNN)*, pp. 1578–1585, 2017.
- Wen, Y., Ma, T., Weng, T.-W., Nguyen, L. M., and Julius, A. A. Abstracted shapes as tokens-a generalizable and interpretable model for time-series classification. In *The Thirty-eighth Annual Conference on Neural Information Processing Systems*, 2024.
- Wen, Y., Ma, T., Luss, R., Bhattacharjya, D., Fokoue, A., and Julius, A. A. Shedding light on time series classification using interpretability gated networks. In *The Thirteenth International Conference on Learning Representations*, 2025.
- Wu, H., Hu, T., Liu, Y., Zhou, H., Wang, J., and Long, M. Timesnet: Temporal 2d-variation modeling for general time series analysis. In *The Eleventh International Conference on Learning Representations*, 2023a.
- Wu, H., Hu, T., Liu, Y., Zhou, H., Wang, J., and Long, M. Timesnet: Temporal 2d-variation modeling for general time series analysis. In *The Eleventh International Conference on Learning Representations*, 2023b.
- Wu, Y., Meng, X., Hu, H., Zhang, J., Dong, Y., and Lu, D. Affirm: Interactive mamba with adaptive fourier filters for long-term time series forecasting. In *Proceedings of the AAAI Conference on Artificial Intelligence*, volume 39, pp. 21599–21607, 2025.
- Ye, L. and Keogh, E. Time series shapelets: a new primitive for data mining. In *Proceedings of the 15th ACM SIGKDD international conference on Knowledge discovery and data mining*, pp. 947–956, 2009.
- Yue, Z., Wang, Y., Duan, J., Yang, T., Huang, C., Tong, Y., and Xu, B. Ts2vec: Towards universal representation of time series. In *Proceedings of the AAAI Conference on Artificial Intelligence*, volume 36, pp. 8980–8987, 2022.
- Zeevi, A., Meir, R., and Adler, R. Time series prediction using mixtures of experts. *Advances in neural information processing systems*, 9, 1996.
- Zerveas, G., Jayaraman, S., Patel, D., Bhamidipaty, A., and Eickhoff, C. A transformer-based framework for multivariate time series representation learning. In *Proceedings of the 27th ACM SIGKDD conference on knowledge discovery & data mining*, pp. 2114–2124, 2021.
- Zhang, K., Wen, Q., Zhang, C., Cai, R., Jin, M., Liu, Y., Zhang, J. Y., Liang, Y., Pang, G., Song, D., et al. Self-supervised learning for time series analysis: Taxonomy, progress, and prospects. *IEEE Transactions on Pattern Analysis and Machine Intelligence*, 2024.
- Zhou, T., Niu, P., Sun, L., Jin, R., et al. One fits all: Power general time series analysis by pretrained lm. *Advances in neural information processing systems*, 36:43322–43355, 2023.
- Zhou, Y., Lei, T., Liu, H., Du, N., Huang, Y., Zhao, V., Dai, A. M., Le, Q. V., Laudon, J., et al. Mixture-of-experts with expert choice routing. *Advances in Neural Information Processing Systems*, 35:7103–7114, 2022.
- Zoph, B., Bello, I., Kumar, S., Du, N., Huang, Y., Dean, J., Shazeer, N., and Fedus, W. St-moe: Designing stable and transferable sparse expert models. *arXiv preprint arXiv:2202.08906*, 2022.



## A. Experimental Setup

### A.1. Datasets

In this study, we employ the UCR time series archive (Dau et al., 2019), a widely recognized benchmark for time series classification tasks (Ismail Fawaz et al., 2019; Middlehurst et al., 2024), to systematically evaluate the effectiveness of the proposed method. This archive encompasses datasets from diverse real-world domains, including human activity recognition, medical diagnostics, and intelligent transportation systems. The UCR archive consists of 128 distinct time series datasets.

As shown in Table 8, many datasets in the UCR archive have a notably greater number of test samples than training samples, such as the *CBF*, *DiatomSizeReduction*, *ECGFiveDays*, *MoteStrain*, and *TwoLeadECG* time series datasets. Moreover, the original UCR time series datasets lack a specific validation set. The limited amount of training samples and the lack of a validation set present challenges in fairly comparing various deep learning-based time series classification methods.

Following the experimental settings outlined in (Ma et al., 2024) and the recommendations of (Dau et al., 2019), we integrate the raw training and test sets and employ a five-fold cross-validation strategy to partition the dataset into training, validation, and test sets in a 3:1:1 ratio. Consistent with the approach in (Ma et al., 2024), each fold is sequentially designated as the test set, while the remaining four folds are randomly divided into training and validation sets in a 3:1 ratio. This cross-validation procedure ensures that each time series sample in the dataset is utilized as a test sample at once, thereby providing a comprehensive evaluation of classifier performance. Consequently, the specific indexing of samples during cross-validation does not substantially influence the final classification results, as each sample contributes to assessing the model’s performance.

### A.2. Baselines

We conduct a comparative analysis of SoftShape against 19 baseline methods. Notably, nine of these baseline deep learning methods are derived from the experimental setting presented in (Ma et al., 2024), including FCN, T-Loss, SelfTime, TS-TCC, TST, TS2Vec, TimesNet, PatchTST, and GPT4TS. While Ma et al. (2024) review a broad range of techniques for time series pre-training, its experimental design for the UCR 128 time series datasets was specifically structured to evaluate the strengths and limitations of these nine deep learning models in the context of supervised time series classification. Therefore, we adopt these nine deep learning methods as baseline models for our experimental analysis, as described below:

- FCN<sup>1</sup> (Wang et al., 2017) employs a three-layer one-dimensional fully convolutional network along with a one-layer global average pooling layer for time series classification.
- T-Loss<sup>2</sup> (Franceschi et al., 2019) utilizes temporal convolutional networks as its foundation and presents an innovative triplet loss for learning representations of time series in the time series classification task.
- SelfTime<sup>3</sup> (Fan et al., 2020) is a framework for time series representation learning that explores both inter-sample and intra-temporal relationships for time series classification tasks.
- TS-TCC<sup>4</sup> (Eldele et al., 2021) is a framework for learning time series representations through temporal and contextual contrasting for classification tasks.
- TST<sup>5</sup> (Zerveas et al., 2021) is a framework for multivariate time series representation learning based on the Transformer architecture for classification tasks.
- TS2Vec<sup>6</sup> (Yue et al., 2022) is a general framework for time series representation learning across various semantic levels, aimed at tasks such as time series classification, forecasting, and anomaly detection. In the context of the time series classification task, the authors utilized temporal convolutional networks (TCN) as the foundational framework, leveraging the low-dimensional feature representation derived from TCN as input for a support vector machine classifier utilizing a radial basis function kernel for the classification process.

<sup>1</sup>[https://github.com/cauchyturing/UCR\\_Time\\_Series\\_Classification\\_Deep\\_Learning\\_Baseline](https://github.com/cauchyturing/UCR_Time_Series_Classification_Deep_Learning_Baseline)

<sup>2</sup><https://github.com/White-Link/UnsupervisedScalableRepresentationLearningTimeSeries>

<sup>3</sup><https://github.com/haoyfan/SelfTime>

<sup>4</sup><https://github.com/emadeldeen24/TS-TCC>

<sup>5</sup>[https://github.com/gzerveas/mvts\\_transformer](https://github.com/gzerveas/mvts_transformer)

<sup>6</sup><https://github.com/yuezhihan/ts2vec>

Table 8: Details of the UCR 128 time series datasets. “Train” represents the count of samples within the raw training set. “Test” represents the count of samples within the raw test set. “Total” represents the overall count of samples within the time series dataset. “Class” indicates the number of classes present within each time series dataset. “Length” refers to the sequence length of the univariate time series within the corresponding dataset. The presence of “Vary” signifies that the dataset includes instances with missing values.

ID	Name	# Train	# Test	# Total	# Class	# Length	ID	Name	# Train	# Test	# Total	# Class	# Length
1	ACSF1	100	100	200	10	1460	65	ItalyPowerDemand	67	1029	1096	2	24
2	Adiac	390	391	781	37	176	66	LargeKitchenAppliances	375	375	750	3	720
3	AllGestureWiimoteX	300	700	1000	10	Vary	67	Lightning2	60	61	121	2	637
4	AllGestureWiimoteY	300	700	1000	10	Vary	68	Lightning7	70	73	143	7	319
5	AllGestureWiimoteZ	300	700	1000	10	Vary	69	Mallat	55	2345	2400	8	1024
6	ArrowHead	36	175	211	3	251	70	Meat	60	60	120	3	448
7	Beef	30	30	60	5	470	71	MedicalImages	381	760	1141	10	99
8	BeetleFly	20	20	40	2	512	72	MelbournePedestrian	1194	2439	3633	10	24
9	BirdChicken	20	20	40	2	512	73	MiddlePhalanxOutlineAgeGroup	400	154	554	3	80
10	BME	30	150	180	3	128	74	MiddlePhalanxOutlineCorrect	600	291	891	2	80
11	Car	60	60	120	4	577	75	MiddlePhalanxTW	399	154	553	6	80
12	CBF	30	900	930	3	128	76	MixedShapesRegularTrain	500	2425	2925	5	1024
13	Chinatown	20	343	363	2	24	77	MixedShapesSmallTrain	100	2425	2525	5	1024
14	ChlorineConcentration	467	3840	4307	3	166	78	MoteStrain	20	1252	1272	2	84
15	CinCECGTorso	40	1380	1420	4	1639	79	NonInvasiveFetalECGThorax1	1800	1965	3765	42	750
16	Coffee	28	28	56	2	286	80	NonInvasiveFetalECGThorax2	1800	1965	3765	42	750
17	Computers	250	250	500	2	720	81	OliveOil	30	30	60	4	570
18	CricketX	390	390	780	12	300	82	OSULeaf	200	242	442	6	427
19	CricketY	390	390	780	12	300	83	PhalangesOutlinesCorrect	1800	858	2658	2	80
20	CricketZ	390	390	780	12	300	84	Phoneme	214	1896	2110	39	1024
21	Crop	7200	16800	24000	24	46	85	PickupGestureWiimoteZ	50	50	100	10	Vary
22	DiatomSizeReduction	16	306	322	4	345	86	PigAirwayPressure	104	208	312	52	2000
23	DistalPhalanxOutlineAgeGroup	400	139	539	3	80	87	PigArtPressure	104	208	312	52	2000
24	DistalPhalanxOutlineCorrect	600	276	876	2	80	88	PigCVP	104	208	312	52	2000
25	DistalPhalanxTW	400	139	539	6	80	89	PLAID	537	537	1074	11	Vary
26	DodgerLoopDay	78	80	158	7	288	90	Plane	105	105	210	7	144
27	DodgerLoopGame	20	138	158	2	288	91	PowerCons	180	180	360	2	144
28	DodgerLoopWeekend	20	138	158	2	288	92	ProximalPhalanxOutlineAgeGroup	400	205	605	3	80
29	Earthquakes	322	139	461	2	512	93	ProximalPhalanxOutlineCorrect	600	291	891	2	80
30	ECG200	100	100	200	2	96	94	ProximalPhalanxTW	400	205	605	6	80
31	ECG5000	500	4500	5000	5	140	95	RefrigerationDevices	375	375	750	3	720
32	ECGFiveDays	23	861	884	2	136	96	Rock	20	50	70	4	2844
33	ElectricDevices	8926	7711	16637	7	96	97	ScreenType	375	375	750	3	720
34	EOGHorizontalSignal	362	362	724	12	1250	98	SemgHandGenderCh2	300	600	900	2	1500
35	EOGVerticalSignal	362	362	724	12	1250	99	SemgHandMovementCh2	450	450	900	6	1500
36	EthanolLevel	504	500	1004	4	1751	100	SemgHandSubjectCh2	450	450	900	5	1500
37	FaceAll	560	1690	2250	14	131	101	ShakeGestureWiimoteZ	50	50	100	10	Vary
38	FaceFour	24	88	112	4	350	102	ShapeletSim	20	180	200	2	500
39	FacesUCR	200	2050	2250	14	131	103	ShapesAll	600	600	1200	60	512
40	FiftyWords	450	455	905	50	270	104	SmallKitchenAppliances	375	375	750	3	720
41	Fish	175	175	350	7	463	105	SmoothSubspace	150	150	300	3	15
42	FordA	3601	1320	4921	2	500	106	SonyAIBORobotSurface1	20	601	621	2	70
43	FordB	3636	810	4446	2	500	107	SonyAIBORobotSurface2	27	953	980	2	65
44	FreezerRegularTrain	150	2850	3000	2	301	108	StarLightCurves	1000	8236	9236	3	1024
45	FreezerSmallTrain	28	2850	2878	2	301	109	Strawberry	613	370	983	2	235
46	Fungi	18	186	204	18	201	110	SwedishLeaf	500	625	1125	15	128
47	GestureMidAirD1	208	130	338	26	Vary	111	Symbols	25	995	1020	6	398
48	GestureMidAirD2	208	130	338	26	Vary	112	SyntheticControl	300	300	600	6	60
49	GestureMidAirD3	208	130	338	26	Vary	113	ToeSegmentation1	40	228	268	2	277
50	GesturePebbleZ1	132	172	304	6	Vary	114	ToeSegmentation2	36	130	166	2	343
51	GesturePebbleZ2	146	158	304	6	Vary	115	Trace	100	100	200	4	275
52	GunPoint	50	150	200	2	150	116	TwoLeadECG	23	1139	1162	2	82
53	GunPointAgeSpan	135	316	451	2	150	117	TwoPatterns	1000	4000	5000	4	128
54	GunPointMaleVersusFemale	135	316	451	2	150	118	UMD	36	144	180	3	150
55	GunPointOldVersusYoung	136	315	451	2	150	119	UWaveGestureLibraryAll	896	3582	4478	8	945
56	Ham	109	105	214	2	431	120	UWaveGestureLibraryX	896	3582	4478	8	315
57	HandOutlines	1000	370	1370	2	2709	121	UWaveGestureLibraryY	896	3582	4478	8	315
58	Haptics	155	308	463	5	1092	122	UWaveGestureLibraryZ	896	3582	4478	8	315
59	Herring	64	64	128	2	512	123	Wafer	1000	6164	7164	2	152
60	HouseTwenty	40	119	159	2	2000	124	Wine	57	54	111	2	234
61	InlineSkate	100	550	650	7	1882	125	WordSynonyms	267	638	905	25	270
62	InsectEPGRegularTrain	62	249	311	3	601	126	Worms	181	77	258	5	900
63	InsectEPGSmallTrain	17	249	266	3	601	127	WormsTwoClass	181	77	258	2	900
64	InsectWingbeatSound	220	1980	2200	11	256	128	Yoga	300	3000	3300	2	426

- TimesNet<sup>7</sup> (Wu et al., 2023b) employs TimesBlock to identify multiple periods and capture temporal 2D variations from transformed 2D tensors using a parameter-efficient inception block for time series modeling.

<sup>7</sup><https://github.com/thuml/TimesNet>

- PatchTST<sup>8</sup> (Nie et al., 2023) segment time series into patches while assuming that channels are independent for multivariate time series forecasting. Considering that GPT4TS (Zhou et al., 2023) has utilised similar patch and channel-independent strategies for time series modeling, we employ only the patch strategy and the channel-independent approach by integrating a transformer for time series classification.
- GPT4TS<sup>9</sup> (Zhou et al., 2023) is a unified framework for time-series modeling that utilises pre-trained large language models. Specifically, GPT4TS adopts the same patch and channel-independent strategies used in PatchTST (Nie et al., 2023) for time series classification tasks.

Furthermore, Middlehurst et al. (2024) conduct a comprehensive analysis of the advantages and limitations of eight categories of time series classification methods: distance-based, feature-based, interval-based, shapelet-based, dictionary-based, convolution-based, deep learning-based, and hybrid-based approaches. However, in their experimental evaluation, Middlehurst et al. (2024) utilize only a training set and a test set, without incorporating a validation set for deep learning-based methods performance assessment.

Specifically, for the selected deep learning-based time series classification methods, Middlehurst et al. (2024) employ the training epoch with the lowest training loss to generate test results. This approach increases the risk of overfitting, as the deep learning model is optimized solely on training data, potentially compromising its generalization capability. Nonetheless, the findings of (Middlehurst et al., 2024) indicate that the deep learning-based InceptionTime (Ismail Fawaz et al., 2020) model achieves superior classification performance. Additionally, experimental results (Middlehurst et al., 2024) demonstrate that HIVE-COTE version 2 (HC2) (Middlehurst et al., 2021), which is a hybrid-based method, MultiROCKET-Hydra (MR-H) (Dempster et al., 2023), a convolution-based method, and RDST, a shapelet-based approach, exhibit strong classification performance.

Given that HC2 is computationally intensive, we select the deep learning-based InceptionTime model along with two non-deep learning methods, MR-H and RDST, as baseline models for our study. The details of these baseline methods are outlined as follows:

- Random Dilated Shapelet Transform (RDST)<sup>10</sup> (Guillaume et al., 2022) is a shapelet-based algorithm that adopts many of the techniques of randomly parameterised convolutional kernels to obtain shapelet features for time series classification.
- MultiROCKET-Hydra (MR-H)<sup>11</sup> (Dempster et al., 2023) is a model that combines dictionary-based and convolution-based models, using competing convolutional kernels and combining key aspects of both Rocket and conventional dictionary methods for time series classification.
- InceptionTime<sup>12</sup> (Ismail Fawaz et al., 2020) is a deep convolutional neural network-based model for time series classification, drawing inspiration from the Inception-v4 architecture.

In recent years, scholars have introduced deep learning models based on convolutional neural networks, transformer architectures, and foundation models for time series classification tasks. For our experimental analysis, we have selected seven recently published methods as baseline models, which are detailed as follows:

- LightTS<sup>13</sup> (Campos et al., 2023) employs model distillation to reduce runtime by ensembling multiple classifiers. It consists of two stages: a teacher phase, where at least ten models (e.g., InceptionTime) are trained, and a student phase that distills their knowledge. Due to the time-intensive nature of the teacher phase, evaluation is limited to 18 selected UCR datasets. Moreover, since LightTS (student) underperforms compared to LightTS (teacher), only the latter’s results are reported.

<sup>8</sup><https://github.com/yuqinie98/PatchTST>

<sup>9</sup><https://github.com/DAMO-DI-ML/NeurIPS2023-One-Fits-All>

<sup>10</sup>[https://github.com/aeon-toolkit/aeon/blob/main/aeon/classification/shapelet\\_based/\\_rdst.py](https://github.com/aeon-toolkit/aeon/blob/main/aeon/classification/shapelet_based/_rdst.py)

<sup>11</sup>[https://github.com/aeon-toolkit/aeon/blob/main/aeon/classification/convolution\\_based/\\_mr\\_hydra.py](https://github.com/aeon-toolkit/aeon/blob/main/aeon/classification/convolution_based/_mr_hydra.py)

<sup>12</sup><https://github.com/timeseriesAI/tsai/blob/main/tsai/models/InceptionTime.py>

<sup>13</sup><https://github.com/d-gcc/LightTS>

- ShapeConv<sup>14</sup> (Qu et al., 2024) introduces an interpretable convolutional layer for time series analysis, where the convolutional kernels are designed to act as shapelets. This convolutional design is inspired by the Shapelet distance, a widely adopted approach in time series classification.
- Shapeformer<sup>15</sup> (Le et al., 2024) is a Shapelet Transformer that combines class-specific and generic transformer modules to effectively capture both types of features. Due to the time-consuming shapelet discovery process in Shapeformer, we evaluate its performance on 18 selected UCR datasets
- ModernTCN<sup>16</sup> (Luo & Wang, 2024) is a pure convolution architecture for time series modeling, which utilizes depthwise convolution and grouped pointwise convolution to learn cross-variable and cross-feature information in a decoupled way.
- TSLANet<sup>17</sup> (Eldele et al., 2024) is a time series lightweight adaptive network, as a universal convolutional model by combining an adaptive spectral block and interactive convolution block using patch-based technologies for time series modeling.
- UniTS<sup>18</sup> (Gao et al., 2024) is a unified pre-trained foundation model for time series, designed to handle various forecasting and classification tasks across diverse datasets. Following the experiments in Table 14 of UniTS, we use the UNITS-SUP×64 model as the baseline.
- Medformer<sup>19</sup> (Wang et al., 2024) is a transformer model designed for medical time series classification that utilizes cross-channel multi-granularity patching, and intra-inter granularity self-attention within and among granularities.

### A.3. Implementation Details

We employ the Adam optimizer with a learning rate of 0.001 and a maximum training epoch of 500. Also, for all baseline method training, we implement a consistent early stopping strategy based on validation set loss values (Ma et al., 2024). For all UCR datasets, we apply a uniform normalization strategy to standardize each time series within the dataset (Ismail Fawaz et al., 2019). For datasets containing missing values, we use the mean of observed values at each specific timestamp across all samples in the training set to impute missing values at corresponding timestamps within the time series samples (Ma et al., 2024). Following (Wang et al., 2017), we set the batch size for model training as  $\min(x_{\text{train}}.\text{shape}[0]/10, 16)$ , where  $x_{\text{train}}.\text{shape}[0]$  represents the number of time series samples in the training set, and  $\min(\cdot)$  denotes the function that selects the minimum value.

From Equation (1) in the main text, the length of time series shapelets,  $m$ , satisfies  $2 \leq m \leq T - 1$ . Directly using subsequences of varying lengths as model inputs significantly increases computational complexity and requires additional preprocessing to standardize input dimensions. To address this, Grabocka et al. (2014); Qu et al. (2024) employ a validation set to select a fixed-length  $m$  of subsequence for shapelet learning, where  $m$  is defined as  $\gamma T$ , with possible values  $\{0.1T, 0.2T, \dots, 0.8T\}$ . This approach reduces the total number of candidate subsequences in Equation (1), thereby lowering computational costs. For patch-based time series classification (Nie et al., 2023; Wang et al., 2024), patch lengths are typically chosen from  $\{4, 8, 16, 24, 32, 48, 64\}$ . Our preliminary experiments indicate that setting shape length  $m$  within this range yields better classification performance. However, due to variations in sequence lengths across UCR 128 datasets, a fixed-length setting may be problematic. For datasets with long sequences, setting  $m = 4$  results in excessive candidate subsequences, while for short sequences, setting  $m = 64$  may eliminate viable subsequences. To balance these issues, we select  $m$  from  $\{4, 8, 16, 24, 32, 48, 64, 0.1T, 0.8T\}$  using the validation set.

Additionally, we set the model depth  $L$  to 2. The number of activated experts  $k$  used for the Mixture of Experts (MoE) router in Equation (6) is set to 1, while the total number of experts  $\hat{C}$  in MoE is defined as the total number of classes in each dataset. The parameter  $\lambda$ , which regulates the learning progression of the loss term in Equation (15), is set to 0.001. The sliding window size  $q$  for extracting subsequences is set to 4. The  $d_{\text{attn}}$  in Equation (3) is set to 8 (Early et al., 2024). The rate  $\eta$  in Equation (5) is set to 50%. To mitigate the issue of inaccurate attention score evaluations for most shapes

<sup>14</sup>[https://openreview.net/attachment?id=O8ouVV8PjF&name=supplementary\\_material](https://openreview.net/attachment?id=O8ouVV8PjF&name=supplementary_material)

<sup>15</sup><https://github.com/xuanmay2701/shapeformer>

<sup>16</sup><https://github.com/luodhhh/ModernTCN>

<sup>17</sup><https://github.com/emadeldeen24/TSLANet>

<sup>18</sup><https://github.com/mims-harvard/UniTS>

<sup>19</sup><https://github.com/dl4mhealth/medformer>



during the initial training phase, the model is warm-up trained for 150 epochs before initiating the soft shape sparsification process. For each UCR time series, we calculate the average test accuracy using five-fold test sets from a single seed. To ensure a fair comparison, we maintain a consistent random seed, as well as standardized dataset preprocessing and partitioning for all baseline methods. For SoftShape and deep learning-based baselines, the same optimizer and learning rate are applied during training, selecting the model with the lowest validation loss for test evaluation. Non-deep learning methods are trained on the training set and evaluated on the test set. Furthermore, for deep learning baselines, except LightTS (Campos et al., 2023), a single model instance is employed without ensembling multiple models initialized differently during both training and evaluation. Like (Ismail Fawaz et al., 2019; Ma et al., 2024), we evaluate performance based on the classification accuracy of the test set. Each experiment is conducted five times with five different random seeds, utilizing the PyTorch 1.12.1 platform and four NVIDIA GeForce RTX 3090 GPUs. The source code for SoftShape is available at <https://github.com/qianlima-lab/SoftShape>.

---

**Algorithm 1** The proposed SoftShape model.
 

---

**Input:** shape embedding layer  $w_{shape}$ , attention head  $w_{attn}$ , soft shape learning block  $w_{block}$ , a classifier  $w_c$ , sparse ratio  $\eta$

**Output:**  $w_{shape}$ ,  $w_{attn}$ ,  $w_{block}$ , and  $w_c$ .

- 1: **Step one:** Obtain all shape embeddings  $\hat{S}_n^m$  through  $w_{shape}$  via Eq. (2);  
Using a norm layer to process  $\hat{S}_n^m$ , denoted as  $norm(\hat{S}_n^m)$ ;
  - 2: **Step two:** Soft shape sparsification using  $norm(\hat{S}_n^m)$  as inputs;  
Calculate the attention score for all shapes via the  $w_{attn}$ ;  
Convert scores in the top  $\eta$  proportion of all shapes into soft shape embeddings via Eq. (4);  
Fuse those with scores below the top  $\eta$  proportion into a single shape embedding via Eq. (5);  
Combine soft shape embeddings and the fused single shape embedding, denoted as  $\tilde{S}_n^m$ ;
  - 3: **Step three:** Intra-Shape and Inter-Shape Learning through  $w_{block}$  using  $\tilde{S}_n^m$  as inputs;  
Using a norm layer to process  $\tilde{S}_n^m$ , denoted as  $norm(\tilde{S}_n^m)$ ;  
Obtain Intra-Shape Embeddings via  $w_{block}$  using Eq. (8), denoted as  $\tilde{S}_{Intra}$ ;  
Obtain Inter-Shape Embeddings via  $w_{block}$  using a shared expert, denoted as  $\tilde{S}_{Inter}$ ;  
Combine  $\tilde{S}_n^m$ ,  $\tilde{S}_{Intra}$ , and  $\tilde{S}_{Inter}$  in a residual way, denoted as  $\tilde{S}_{out} = \tilde{S}_n^m + \tilde{S}_{Intra} + \tilde{S}_{Inter}$ ;
  - 4: **Step four:** Set model depth to  $L$  for training by rerunning Step two and Step three  $L$  times using  $\tilde{S}_{out}$  as inputs, denoted the end outputs as  $O_n^m$ ;
  - 5: **Step five:** Classification training using  $O_n^m$  as inputs;  
Update  $w_{shape}$ ,  $w_{attn}$ ,  $w_{block}$ ,  $w_c$  via training objective  $\mathcal{L}_{total}$  using Eq. (15);
- 

## B. Details of Experimental Results

### B.1. Main Results

The test classification accuracy results of SoftShape and 17 baseline methods on the UCR 128 time series dataset are presented in Table 9. Specifically, the test classification accuracy results of nine methods, including FCN, T-Loss, SelfTime, TS-TCC, TST, TS2Vec, TimesNet, PatchTST, and GPT4TS, are obtained from (Ma et al., 2024). Figure 6 illustrates the critical difference diagram and significance analysis results for SoftShape and the 17 baseline methods on the UCR 128 time series dataset. Additionally, Table 10 presents the detailed test classification accuracies of LightTS, Shapeformer, and SoftShape on the selected 18 UCR datasets.

Table 9: The detailed test classification accuracy comparisons on 128 UCR time series datasets. Among these, *Incep* refers to the InceptionTime method, and *MoTCN* refers to the ModernTCN method. The best results are in **bold**.

ID	Dataset	FCN	T-Loss	Selftime	TS-TCC	TST	TS2Vec	TimesNet	PatchTST	GPT4TS	RDST	MR-H	Incep	ShapeConv	MoTCN	TSNet	UniTS	Medformer	SoftShape
1	ACSF1	0.6250	0.8050	0.7250	0.5700	0.7050	0.8800	0.6000	0.7600	0.6200	0.8400	0.8450	0.9050	0.6000	0.4500	0.8700	0.8300	0.8350	<b>0.9100</b>
2	Adiac	0.6492	0.7811	0.7322	0.4003	0.7363	0.8066	0.8082	0.8358	0.8069	0.7848	0.8527	0.9354	0.5635	0.8580	0.8837	0.6596	0.8364	<b>0.9374</b>
3	AllGestureWX.	0.7110	0.7170	0.6461	0.7201	0.5280	0.7820	0.5120	0.5730	0.7220	0.7930	0.8050	0.8540	0.3170	0.7260	0.8970	0.8530	0.6130	<b>0.8980</b>
4	AllGestureWY.	0.6740	0.8110	0.7170	0.7615	0.3850	0.8400	0.5820	0.6730	0.7800	0.8360	0.8770	0.9140	0.2990	0.7470	<b>0.9180</b>	0.8690	0.8250	0.9110
5	AllGestureWZ.	0.7200	0.7470	0.6485	0.6567	0.4780	0.7730	0.6620	0.5890	0.7300	0.7850	0.8100	0.8920	0.3070	0.6540	<b>0.9010</b>	0.8460	0.7250	0.8850
6	ArrowHead	0.8958	0.8770	0.8155	0.8200	0.8722	0.8908	0.7821	0.7078	0.8348	0.9382	0.9430	0.9288	0.6638	0.8152	<b>0.9672</b>	0.9433	0.9434	0.9435
7	Beef	0.8250	0.8750	0.5167	0.6333	0.6667	0.6833	0.8000	0.4167	<b>0.9333</b>	0.8333	0.8500	0.7833	0.6833	0.8500	0.7500	0.7167	0.8333	0.8667
8	BeetleFly	0.9250	<b>0.9750</b>	0.8000	0.6250	0.6750	0.9250	0.7000	0.8500	0.7250	0.9000	0.9250	0.8500	0.9250	0.7500	<b>0.9750</b>	0.8750	0.9000	<b>0.9750</b>
9	BirdChicken	0.7833	<b>0.9833</b>	0.9000	0.6750	0.8500	0.9750	0.8250	0.8500	0.7500	0.9000	0.9000	0.9500	0.9500	0.8250	0.8750	0.8250	0.8250	0.9000
10	BME	0.6000	0.5333	0.9722	0.9889	0.9722	0.9944	0.9778	0.9500	0.9611	<b>1.0000</b>	<b>1.0000</b>	<b>1.0000</b>	0.6722	0.9833	<b>1.0000</b>	0.9889	<b>1.0000</b>	0.9944

# Learning Soft Sparse Shapes for Efficient Time-Series Classification

ID	Dataset	FCN	T-Loss	Selftime	TS-TCC	TST	TS2Vec	TimesNet	PatchTST	GPT4TS	RDST	MR-H	Incep	ShapeConv	MoTCN	TSLANet	UniTS	Medformer	SoftShape
11	Car	<b>1.0000</b>	<b>1.0000</b>	0.6583	0.7167	0.7583	0.8833	0.8417	0.9083	0.9000	0.9500	0.9583	0.9583	0.7750	0.8250	0.9500	0.9078	0.8417	0.9583
12	CBF	0.9417	0.8250	0.9936	0.9967	0.9946	<b>1.0000</b>	<b>1.0000</b>	<b>1.0000</b>	0.9978	<b>1.0000</b>	<b>1.0000</b>	<b>1.0000</b>	0.9989	<b>1.0000</b>	<b>1.0000</b>	0.9983	<b>1.0000</b>	<b>1.0000</b>
13	Chinatown	0.9753	0.9807	0.9669	0.9507	0.9699	0.9726	0.9863	0.9836	0.9863	0.9699	0.9808	0.9836	0.9123	0.9233	0.9863	0.9781	0.9863	<b>0.9890</b>
14	ChlorineCon.	0.9984	0.9988	0.6116	0.8424	0.9974	<b>0.9998</b>	0.9993	0.9995	<b>0.9998</b>	0.9886	0.9954	0.9993	0.6973	0.9991	0.9988	0.9988	0.6427	0.9988
15	CinCECGTorso	0.9986	0.9944	0.9877	0.9995	0.9993	0.9972	0.9930	<b>1.0000</b>	0.9930	<b>1.0000</b>	<b>1.0000</b>	0.9923	0.9789	0.9993	<b>1.0000</b>	0.9958	0.9986	<b>1.0000</b>
16	Coffee	<b>1.0000</b>	0.9818	0.9273	0.9455	0.8758	<b>1.0000</b>	<b>1.0000</b>	<b>1.0000</b>	<b>1.0000</b>	<b>1.0000</b>	<b>1.0000</b>	<b>1.0000</b>	0.9667	<b>1.0000</b>	<b>1.0000</b>	<b>1.0000</b>	0.9818	<b>1.0000</b>
17	Computers	0.8800	0.7140	0.7920	0.6080	0.6880	0.6940	0.8120	0.8380	0.8080	0.8180	0.8540	0.8420	0.6660	0.6540	<b>0.8920</b>	0.8120	0.8280	0.8160
18	CricketX	0.9064	0.7795	0.7316	0.7327	0.7026	0.8321	0.7974	0.7821	0.7910	0.8628	0.8628	0.9013	0.8179	0.7231	0.9205	0.8923	0.8397	<b>0.9321</b>
19	CricketY	0.9000	0.7487	0.6904	0.7161	0.6962	0.8256	0.7808	0.7821	0.8026	0.8436	0.8487	0.8923	0.7692	0.7513	0.8987	0.8808	0.8500	<b>0.9154</b>
20	CricketZ	0.8833	0.7833	0.7411	0.7384	0.6936	0.8487	0.7962	0.7923	0.8026	0.8692	0.8526	0.8679	0.7744	0.7385	0.9064	0.8859	0.8564	<b>0.9372</b>
21	Crop	0.1312	0.7063	0.6634	0.7801	0.7709	0.7448	0.8503	0.1193	0.8764	0.7675	0.7805	0.8757	0.1833	0.0922	0.5781	0.0417	0.3043	<b>0.8765</b>
22	DiatomSizeRe.	0.9969	0.9969	0.9723	0.9783	<b>1.0000</b>	0.9969	0.9938	<b>1.0000</b>	0.9907	<b>1.0000</b>	<b>1.0000</b>	0.9969	0.9531	0.9877	0.9969	0.9719	0.9938	<b>1.0000</b>
23	DistalPhalanxOut.	0.9091	0.8274	0.7959	0.8200	0.8404	0.8125	0.8590	0.8779	0.8890	0.8311	0.8329	0.8850	0.7662	0.8089	0.9333	0.8070	0.8312	<b>0.9518</b>
24	DistalPhalanxOut.	0.8917	0.8471	0.7895	0.7646	0.8254	0.8185	0.8860	0.9009	0.8929	0.8323	0.8448	0.8802	0.7980	0.7752	0.9018	0.7363	0.6529	<b>0.9054</b>
25	DistalPhalanxTW	0.8423	0.7421	0.7514	0.7755	0.7551	0.7792	0.8499	0.8485	0.8263	0.7866	0.7700	0.8500	0.7421	0.7979	0.8796	0.7718	0.8349	<b>0.9037</b>
26	DodgerLoopDay	0.7486	0.4819	0.4742	0.5885	0.5377	0.6391	0.7107	0.6694	0.7403	0.6266	0.5315	0.7681	0.7871	0.5528	0.8244	<b>0.8750</b>	0.8621	0.8623
27	DodgerLoopGame	0.8167	0.8921	0.8282	0.8857	0.8988	0.9563	0.8484	0.8872	0.9001	0.9179	0.9175	<b>0.9621</b>	0.9373	0.7966	0.9563	0.8484	0.9242	0.9433
28	DodgerLoopWeek.	0.9812	0.9677	0.9681	0.9742	0.9679	0.9812	0.9688	0.9492	0.9165	0.9746	0.9873	0.9806	0.9937	0.9937	0.9873	0.9806	<b>1.0000</b>	<b>1.0000</b>
29	Earthquakes	0.7376	0.7417	0.7983	0.7505	0.7961	0.7983	0.9136	0.9115	0.9052	0.7809	0.7939	0.7939	0.8526	0.7333	<b>0.9222</b>	0.8613	0.8963	0.8917
30	ECG200	0.8482	0.7983	0.7900	0.7950	0.8600	0.8800	0.9100	0.8763	0.8951	0.9200	0.9250	0.9250	0.8600	0.9050	0.9450	0.8850	0.9100	<b>0.9475</b>
31	ECG5000	0.9350	0.8500	0.9317	0.9525	0.9502	0.9528	0.9708	0.9364	0.9746	0.9552	0.9566	0.9750	0.9432	0.5510	0.9760	0.9622	0.9460	<b>0.9796</b>
32	ECGFiveDays	0.9258	0.9478	0.9873	0.9972	0.9977	<b>1.0000</b>	<b>1.0000</b>	<b>1.0000</b>	0.9978	<b>1.0000</b>	<b>1.0000</b>	<b>1.0000</b>	0.9636	<b>1.0000</b>	<b>1.0000</b>	<b>1.0000</b>	<b>1.0000</b>	<b>1.0000</b>
33	ElectricDevices	0.6519	0.6547	0.7173	0.8639	0.8758	0.8848	0.8610	0.4883	0.8610	0.9024	0.9094	<b>0.9459</b>	0.7259	0.3500	0.8991	0.7921	0.7665	0.9208
34	EOGHorizontalS.	<b>1.0000</b>	<b>1.0000</b>	0.7579	0.6295	0.6781	0.7279	0.6092	0.8010	0.7581	0.7942	0.8453	0.8910	0.7056	0.7281	0.8993	0.8469	0.8344	0.9007
35	EOGVerticalS.	0.6731	0.8736	0.6774	0.6190	0.4806	0.6519	0.6369	0.8013	0.7804	0.7335	0.7984	0.8703	0.4764	0.6922	<b>0.8965</b>	0.8620	0.8220	0.8814
36	EthanolLevel	0.8307	0.5627	0.4864	0.2985	0.7919	0.5897	0.7690	0.7248	0.8337	0.7480	0.7261	0.9144	0.2929	<b>0.9522</b>	0.9184	0.4771	0.8019	0.9204
37	FaceAll	0.9462	0.9720	0.9552	0.9914	0.9720	0.9871	0.9733	0.8057	0.9877	0.9951	0.9951	0.9973	0.9520	0.9324	0.9947	0.9880	0.9778	<b>0.9978</b>
38	FaceFour	0.9557	0.9281	0.8830	0.9379	0.9375	0.9640	0.9557	0.9068	0.9826	<b>1.0000</b>	0.9909	<b>1.0000</b>	<b>1.0000</b>	0.9826	0.9913	0.9735	0.9826	0.9909
39	FacesUCR	0.9969	0.9729	0.9544	0.9899	0.9702	0.9902	0.9800	0.9824	0.9796	0.9938	0.9938	<b>0.9973</b>	0.9653	0.9840	0.9960	0.9889	0.9831	0.9956
40	FiftyWords	0.5072	0.8088	0.6705	0.7628	0.7381	0.8022	0.8276	0.8417	0.7709	0.8619	0.8718	0.9315	0.8674	0.8718	0.9249	0.8807	0.8685	<b>0.9359</b>
41	Fish	0.9686	0.8743	0.8514	0.8114	0.8628	0.9343	0.8000	0.9343	0.9143	0.9857	0.9829	<b>0.9943</b>	0.8371	0.8800	0.9629	0.9400	0.9086	0.9771
42	FordA	0.9734	0.9114	0.8787	0.9342	0.8990	0.9303	0.9348	0.9500	0.9403	0.9484	0.9537	0.9728	0.8935	0.9590	0.9740	0.9718	0.8450	<b>0.9772</b>
43	FordB	0.9312	0.9035	0.8771	0.9087	0.8650	0.9132	0.9046	0.9377	0.9287	0.9327	0.9345	0.9705	0.8934	0.9476	0.9658	0.9328	0.8488	<b>0.9744</b>
44	FreezerRegular.	0.9790	0.9980	0.9974	0.9969	0.9987	0.9977	0.9990	0.9393	0.9987	0.9993	<b>0.9997</b>	0.9993	0.7590	0.6967	0.9993	0.8100	0.6950	0.9990
45	FreezerSmall.	0.8359	0.9965	0.9975	0.9966	0.9979	0.9969	0.9969	0.8492	0.9983	0.9993	<b>0.9997</b>	0.9986	0.7575	0.5209	<b>0.9997</b>	0.9396	0.8351	0.9990
46	Fungi	0.9118	<b>1.0000</b>	0.9316	0.9557	0.9902	<b>1.0000</b>	0.8337	0.7276	0.9049	<b>1.0000</b>	<b>1.0000</b>	<b>1.0000</b>	0.9951	0.9415	<b>1.0000</b>	<b>1.0000</b>	0.9902	<b>1.0000</b>
47	GestureMidAirD1	0.6954	0.5919	0.7067	0.6120	0.6181	0.6479	0.6099	0.6103	0.6449	0.7452	0.7632	0.7786	0.6810	0.7074	0.8493	0.8051	0.7813	<b>0.8640</b>
48	GestureMidAirD2	0.5860	0.4973	0.5504	0.4853	0.5475	0.5270	0.5449	0.5692	0.5410	0.5859	0.5858	0.7606	0.5481	0.6308	0.7640	0.7287	0.7079	<b>0.7962</b>
49	GestureMidAirD3	0.3819	0.3108	0.3664	0.3137	0.3462	0.3315	0.4559	0.4962	0.5282	0.4144	0.4291	0.6104	0.5364	0.5399	0.6577	0.6343	0.6094	<b>0.7613</b>
50	GesturePebbleZ1	0.9541	0.6420	0.9043	0.8977	0.7761	0.9507	0.9541	0.8316	0.9158	0.9476	0.9703	0.9836	0.8289	0.9177	<b>0.9967</b>	0.9573	0.9729	0.9867
51	GesturePebbleZ2	0.9343	0.6614	0.8817	0.8914	0.8159	0.9473	0.8850	0.7800	0.9382	0.9606	0.9540	<b>0.9836</b>	0.8127	0.9475	0.9738	0.9606	0.9409	<b>0.9836</b>
52	GunPoint	<b>1.0000</b>	0.9850	0.9550	0.9500	0.9700	0.9950	0.9850	0.9800	0.9800	<b>1.0000</b>	<b>1.0000</b>	<b>1.0000</b>	0.9350	0.9600	0.9900	0.9400	0.9800	0.9900
53	GunPointAgeSpan	0.9956	0.9756	0.9800	0.9578	0.9778	0.9889	0.9823	0.9889	0.9890	0.9956	<b>1.0000</b>	0.9889	0.9157	0.8024	0.9890	0.9179	0.9911	0.9868
54	GunPointMale.	0.9978	0.9911	0.9845	0.9823	0.9867	0.9956	0.9956	<b>1.0000</b>	0.9956	<b>1.0000</b>	<b>1.0000</b>	0.9933	0.9712	0.9845	0.9934	0.9845	0.9934	0.9956
55	GunPointOld.	0.9934	0.9468	0.9490	0.9512	0.9667	0.9956	0.9800	0.9912	0.9691	0.9956	<b>0.9978</b>	0.9712	0.7653	0.9180	0.9823	0.9623	0.9712	0.9779
56	Ham	0.6632	0.8080	0.7193	0.8275	0.8450	0.8741	0.9023	0.5420	<b>0.9349</b>	0.9064	0.8740	0.8461	0.6783	0.8458	0.8972	0.8788	0.9207	0.9161
57	HandOutlines	0.8956	0.9073	0.8425	0.8657	0.7170	0.9168	0.9029	0.9350	0.8956	0.9482	0.9482	0.9606	0.6934	<b>0.9701</b>	0.9460	0.9336	0.9131	0.9533
58	Haptics	0.6158	0.4879	0.4730	0.4990	0.4794	0.5594	0.6422	0.6672	0.6842	0.6241	0.5983	0.6960	0.5033	0.5862	0.6961	0.4899	0.6355	<b>0.7522</b>
59	Herring	0.6406	0.5929	0.6086	0.5452	0.6400	0.6806	0.6560	0.7604	0.8003	0.6868	0.6554	0.7185	0.6649	0.5791	<b>0.8212</b>	0.6554	0.7046	0.7671
60	HouseTwenty	<b>0.9875</b>	0.8935	0.9746	0.8244	0.7673	0.9496	0.8615	0.8617	0.8683	0.9750	<b>0.9875</b>	0.9500	0.9623	0.7429	0.9500	0.9121	0.9496	0.9688
61	InlineSkate	0.7046	0.6354	0.1922	0.4172	0.4754	0.6415	0.5369	<b>0.8985</b>	0.6499	0.6508	0.7354	0.7554	0.6446	0.6431	0.7769	0.5308	0.7662	0.8077
62	InsectEPGR.	0.9935	0.9839	0.9616	0.8554	0.8327	0.9807	0.8267	0.9617	0.8307	<b>1.0000</b>	<b>1.0000</b>	<b>1.0000</b>	0.7945	0.7818	0.9904	0.8779	0.9808	0.9968
63	InsectEPGWS.	0.8761	0.9850	0.9774	0.8308	0.8235	0.9699	0.8011	0.9511	0.8198	<b>1.0000</b>	<b>1.0000</b>	0.9963	0.7973	0.8234	0.9813	0.9064	0.9514	0.9963
64	InsectWing.	0.7309	0.6673	0.6092	0.7119	0.6982	0.7077	0.7355	0.8609	0.8518	0.7286	0.730							

## Learning Soft Sparse Shapes for Efficient Time-Series Classification

ID	Dataset	FCN	T-Loss	Selftime	TS-TCC	TST	TS2Vec	TimesNet	PatchTST	GPT4TS	RDST	MR-H	Incep	ShapeConv	MoTCN	TSLANet	UniTS	Medformer	SoftShape
101	ShakeWimoteZ.	0.9200	0.9100	0.8900	0.8500	0.6800	0.9300	0.5900	0.6900	0.7200	0.9200	0.9300	0.9600	0.8700	0.7400	0.9500	0.8400	0.8300	<b>0.9800</b>
102	ShapeletSim	0.9700	0.9200	0.9450	0.6050	0.5600	0.9850	0.5500	0.9150	0.6300	<b>1.0000</b>	<b>1.0000</b>	<b>1.0000</b>	0.8300	0.6450	<b>1.0000</b>	0.9800	0.8850	0.9950
103	ShapesAll	0.7267	0.8925	0.8835	0.7777	0.7292	0.9133	0.8325	0.8833	0.8500	0.9417	0.9533	<b>0.9583</b>	0.8225	0.8950	0.9083	0.9192	0.8617	0.9575
104	SmallAppliances.	0.7987	0.7227	0.8256	0.7095	0.5747	0.7347	0.7840	0.6387	0.7213	0.8133	0.8333	0.9008	0.5413	0.6573	0.9040	0.7840	0.8173	<b>0.9053</b>
105	SmoothSubspace	0.9467	0.9233	0.9367	0.9433	0.9800	0.9633	0.9767	0.9633	0.9133	<b>0.9900</b>	0.9833	0.9800	0.9433	0.8567	0.9567	0.9400	0.9733	0.9867
106	SonyAISurface1.	0.9984	0.9920	0.9726	0.9775	0.9823	0.9952	0.9952	0.9888	0.9888	0.9984	<b>1.0000</b>	0.9984	0.9646	0.9936	0.9904	0.9888	0.9823	0.9936
107	SonyAISurface2.	0.9990	0.9878	0.9376	0.9849	0.9847	0.9949	0.9939	0.9939	0.9949	0.9980	0.9990	<b>1.0000</b>	0.8990	0.9847	0.9969	0.9867	0.9837	0.9980
108	StarLightCurves	0.9803	0.9783	0.9793	0.9738	0.9734	0.9801	0.9616	<b>0.9912</b>	0.9818	0.9827	0.9838	0.9903	0.9686	0.9892	0.9910	0.9675	0.9694	0.9905
109	Strawberry	0.9756	0.9614	0.9426	0.9414	0.9735	0.9685	0.9766	0.9624	0.9736	0.9786	0.9797	0.9797	0.8790	0.9542	0.9817	0.9532	0.9054	<b>0.9868</b>
110	SwedishLeaf	<b>0.9929</b>	0.9404	0.9158	0.9423	0.9253	0.9502	0.9449	0.9778	0.9671	0.9707	0.9751	0.9849	0.9250	0.9618	0.9893	0.9760	0.9689	0.9867
111	Symbols	<b>0.9961</b>	0.9824	0.9798	0.9733	0.9765	0.9863	0.9618	0.9922	0.9667	0.9951	0.9951	<b>0.9961</b>	0.9686	0.9765	0.9833	0.9471	0.9745	0.9941
112	SyntheticControl	0.9700	0.9883	0.9683	0.9950	0.9767	0.9983	0.9767	0.9700	0.9717	0.9933	0.9933	<b>1.0000</b>	0.9783	0.9400	0.9967	0.9933	0.9900	0.9967
113	ToeSegmentation1	0.9664	0.9551	0.9143	0.9181	0.6903	0.9588	0.8514	0.9219	0.8846	0.9776	0.9776	0.9812	0.9293	0.6761	0.9778	0.7500	0.8771	<b>0.9852</b>
114	ToeSegmentation2	0.9282	0.9219	0.9283	0.8250	0.8435	0.9517	0.8316	0.8510	0.8143	0.9638	0.9517	0.9704	0.9706	0.8561	0.9522	0.9045	0.8554	<b>0.9882</b>
115	Trace	<b>1.0000</b>	<b>1.0000</b>	0.9950	0.9150	0.9700	<b>1.0000</b>	0.9400	<b>1.0000</b>	0.8900	<b>1.0000</b>	<b>1.0000</b>	<b>1.0000</b>	<b>1.0000</b>	0.9800	<b>1.0000</b>	0.8100	<b>1.0000</b>	<b>1.0000</b>
116	TwoLeadECG	<b>1.0000</b>	0.9983	0.9932	0.9965	0.9914	0.9991	0.9983	0.9991	0.9948	0.9991	<b>1.0000</b>	<b>1.0000</b>	0.8615	0.9983	0.9991	0.9991	0.9974	<b>1.0000</b>
117	TwoPatterns	0.9454	<b>1.0000</b>	0.9513	0.9990	0.9994	<b>1.0000</b>	0.9980	0.9990	0.9962	<b>1.0000</b>	<b>1.0000</b>	<b>1.0000</b>	0.9944	<b>1.0000</b>	0.9998	0.9994	0.9986	<b>1.0000</b>
118	UMD	0.8778	0.9944	0.9389	0.9611	0.9778	0.9944	0.9833	<b>1.0000</b>	0.9778	<b>1.0000</b>	0.9944	<b>1.0000</b>	0.9056	<b>1.0000</b>	0.9944	0.9833	<b>1.0000</b>	0.9944
119	UWaveGestureAll.	0.9245	0.9518	0.8595	0.9750	0.9602	0.9652	0.9504	<b>0.9913</b>	0.9708	0.9882	0.9897	0.9812	0.9252	0.9888	<b>0.9913</b>	0.9795	0.9757	0.9900
120	UWaveGestureX.	0.8665	0.8457	0.6680	0.8385	0.8091	0.8513	0.8924	0.9214	0.9002	0.8803	0.9015	0.9196	0.7977	0.9216	0.9413	<b>0.9458</b>	0.9219	0.9406
121	UWaveGestureY.	0.7906	0.7887	0.5342	0.7573	0.7300	0.7874	0.8455	0.8955	0.8399	0.8109	0.8481	0.8850	0.6936	0.8828	<b>0.9194</b>	0.9100	0.8777	0.9109
122	UWaveGestureZ.	0.8484	0.8021	0.6076	0.7762	0.4790	0.8024	0.8669	0.9006	0.8535	0.8314	0.8584	0.8812	0.7693	0.8781	<b>0.9219</b>	0.9143	0.8785	0.9170
123	Wafer	<b>1.0000</b>	0.9989	0.9587	0.9982	0.9992	0.9990	0.9986	0.9992	0.9992	<b>1.0000</b>	<b>1.0000</b>	0.9999	0.9785	0.9993	0.9999	0.9994	0.9971	<b>1.0000</b>
124	Wine	0.5411	0.9553	0.6743	0.5221	0.5854	<b>0.9648</b>	0.8289	0.5135	0.8561	0.9553	0.9644	0.7593	0.5490	0.5043	0.7494	0.4953	0.5130	0.8842
125	WordSynonyms	0.5967	0.8022	0.5718	0.7444	0.7083	0.7989	0.8442	0.8690	0.7823	0.8575	0.8740	<b>0.9315</b>	0.8254	0.8431	0.8928	0.8762	0.8486	0.9175
126	Worms	0.7906	0.6821	0.6860	0.5423	0.4148	0.7210	0.7446	0.8072	0.7097	0.7051	0.7357	0.8181	0.5856	0.5236	0.8429	0.7800	0.7876	<b>0.8453</b>
127	WormsTwoClass	0.8025	0.7634	0.7557	0.6898	0.6240	0.7716	0.7833	<b>0.9037</b>	0.8221	0.7715	0.7753	0.7983	0.6710	0.6906	0.8692	0.8414	0.8376	0.8802
128	Yoga	0.9718	0.9661	0.7699	0.9207	0.9497	0.9709	0.9539	0.9739	0.9476	0.9842	0.9906	<b>0.9933</b>	0.7661	0.9845	0.9694	0.8970	0.9718	0.9830
Avg. Acc		0.8296	0.8325	0.8017	0.7807	0.7755	0.8691	0.8367	0.8265	0.8593	0.8897	0.8972	0.9181	0.7688	0.7938	0.9205	0.8502	0.8541	<b>0.9334</b>
Avg. Rank		9.53	11.12	13.80	13.96	13.54	8.43	10.13	9.56	9.34	6.41	5.51	4.05	13.91	11.37	3.68	9.66	9.26	<b>2.72</b>
Win		13	9	0	0	1	9	7	12	6	23	29	29	5	9	31	5	7	<b>53</b>

Table 10: The detailed test classification accuracy of LightTS, Shapeformer, and SoftShape on 18 UCR datasets.

Dataset	LightTS	Shapeformer	SoftShape (Ours)
ArrowHead	<b>0.9480</b>	0.8439	0.9435
CBF	<b>1.0000</b>	0.9978	<b>1.0000</b>
CricketX	0.9282	0.6564	<b>0.9321</b>
DistalPhalanxOutlineAgeGroup	0.8664	0.7921	<b>0.9518</b>
DistalPhalanxOutlineCorrect	0.8460	0.8151	<b>0.9054</b>
ECG5000	0.9630	0.9166	<b>0.9796</b>
EOGVerticalSignal	0.7737	0.5635	<b>0.9007</b>
EthanolLevel	0.9044	0.7261	<b>0.9204</b>
Fish	<b>0.9800</b>	0.9114	0.9771
GunPoint	0.9850	<b>0.9900</b>	<b>0.9900</b>
InsectWingbeatSound	0.8300	0.6586	<b>0.8882</b>
ItalyPowerDemand	0.9708	0.9690	<b>0.9891</b>
MelbournePedestrian	<b>0.9879</b>	0.7134	0.9573
MiddlePhalanxTW	0.7673	0.6293	<b>0.8376</b>
MixedShapesRegularTrain	<b>0.9795</b>	0.8055	0.9757
OSULeaf	<b>0.9523</b>	0.7649	0.9504
Trace	<b>1.0000</b>	<b>1.0000</b>	<b>1.0000</b>
WordSynonyms	0.8892	0.6773	<b>0.9161</b>
Avg. Acc	0.9207	0.8017	<b>0.9453</b>
Avg. Rank	1.67	2.78	<b>1.28</b>
Win	7	2	<b>13</b>
P-value	8.91E-03	9.80E-06	-

## B.2. Ablation Study

Table 11 presents the detailed test classification accuracy results for various ablation components of SoftShape across 128 UCR time series datasets.

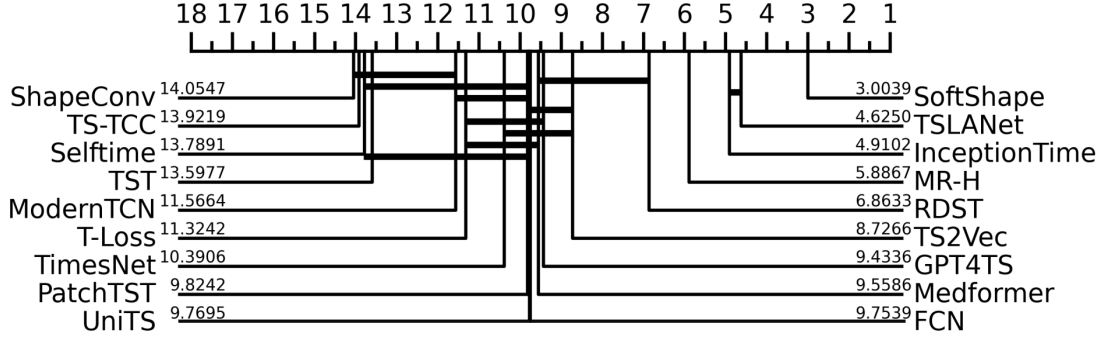


Figure 6: The critical diagram (CD) (Demšar, 2006) illustrates statistical testing comparisons between SoftShape and baseline methods on the 128 UCR time series datasets. A smaller CD value indicates better method performance. The absence of a connecting line between the two methods signifies a statistically significant performance difference.

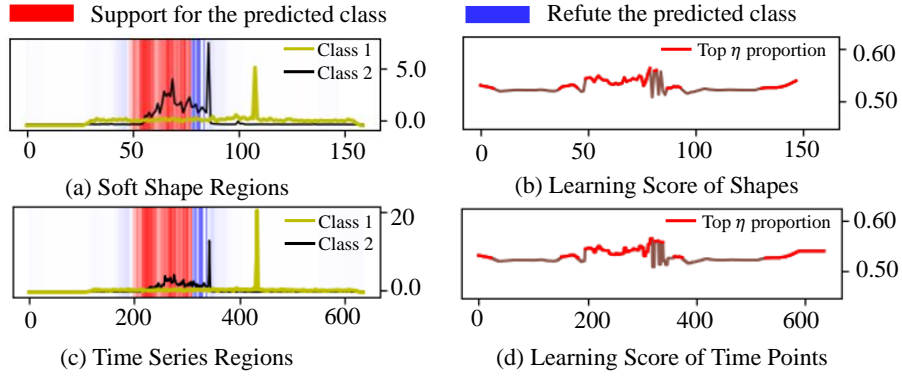


Figure 7: The MIL visualization on the *Lightning2* dataset.

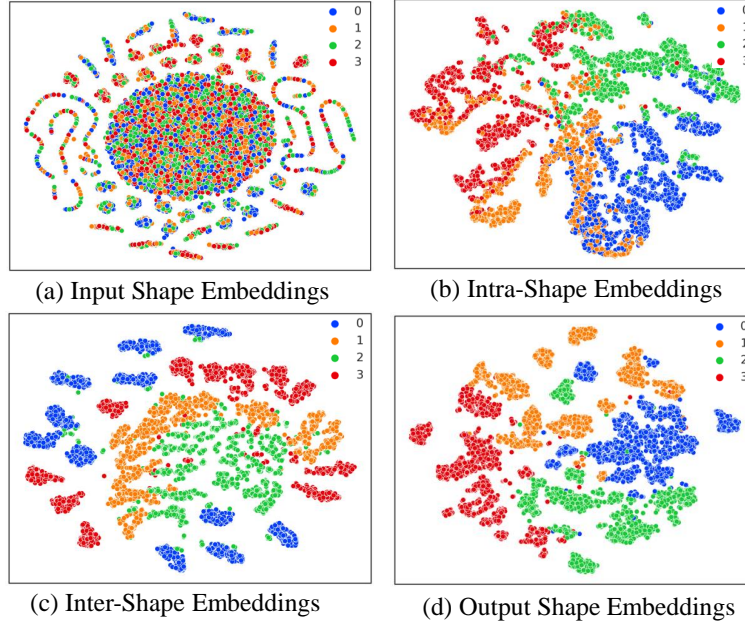
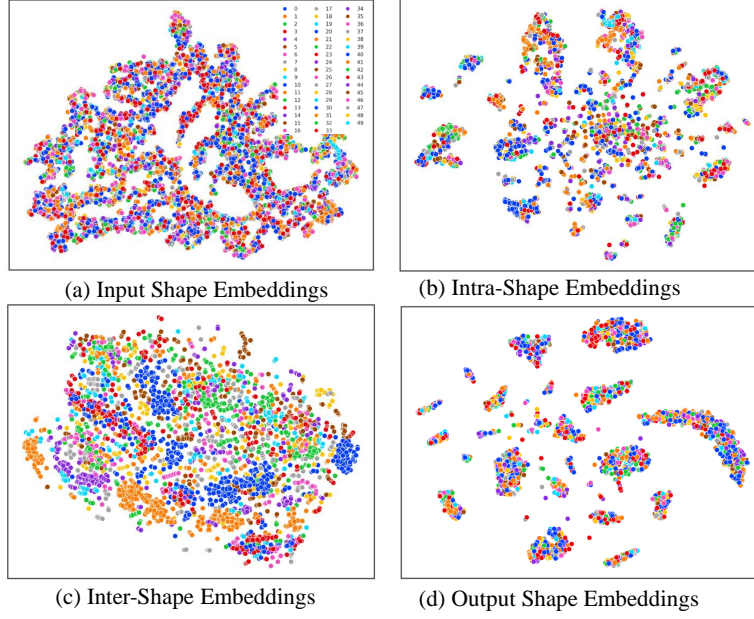
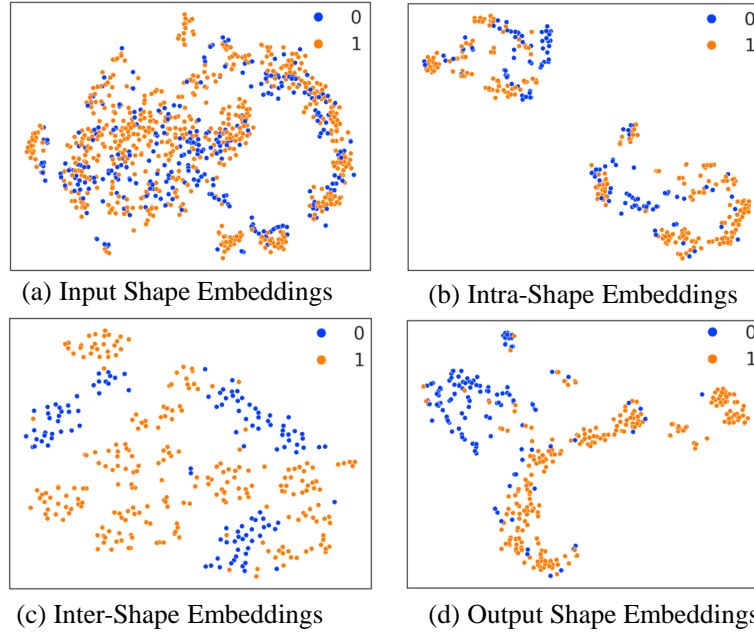


Figure 8: The t-SNE visualization on the *TwoPatterns* dataset.




 Figure 9: The t-SNE visualization on the *Fiftywords* dataset.

 Figure 10: The t-SNE visualization on the *ECG200* dataset.

### B.3. Shape Sparsification and Learning Analysis

Due to the considerable time requirements for conducting experimental evaluations on all 128 UCR time series datasets for some baselines and hyperparameter analysis, 18 datasets were chosen from the 128 UCR datasets based on four key criteria: the number of samples, the length of the sample sequences, the number of classes, and the relevance to various application scenarios. Specifically, these 18 datasets vary in sample size from 200 to 5000, in sequence length from 24 to 1751, and in classes from 2 to 25. Besides, the selected datasets cover diverse application areas, including handwritten font sequence recognition (e.g., the *WordSynonyms* dataset), human activity recognition (e.g., the *CricketX* dataset), and medical diagnosis

Table 11: The detailed test classification accuracy of the ablation study on 128 UCR datasets. Among these, *w/o II* refers to the *w/o Intra & Inter* method. The best results are in **bold**.

ID	Dataset	SoftShape	w/o Soft	w/o Intra	w/o Inter	w/o II	with Linear	ID	Dataset	SoftShape	w/o Soft	w/o Intra	w/o Inter	w/o II	with Linear
1	ACSF1	<b>0.9100</b>	0.8700	0.8150	0.8900	0.8700	0.8850	67	Lightning2	0.8857	<b>0.9110</b>	0.8819	0.9033	0.8450	0.9023
2	Adiac	<b>0.9374</b>	0.8810	0.9297	0.8274	0.8094	0.9259	68	Lightning7	0.8966	0.9308	<b>0.9517</b>	0.8997	0.9101	0.8894
3	AllGestureWX.	<b>0.8980</b>	0.8680	0.8970	0.8040	0.5850	0.8620	69	Mallat	0.9988	<b>1.0000</b>	<b>1.0000</b>	0.9996	0.9992	0.9996
4	AllGestureWY.	<b>0.9110</b>	0.9030	0.9080	0.8360	0.6260	0.8930	70	Meat	0.9917	<b>1.0000</b>	0.9917	0.9917	0.9917	<b>1.0000</b>
5	AllGestureWZ.	<b>0.8850</b>	0.8350	0.8786	0.8080	0.5960	0.8750	71	MedicalImages	0.9213	0.9221	0.9204	0.9134	0.7783	<b>0.9256</b>
6	ArrowHead	0.9435	0.9672	<b>0.9765</b>	0.9627	0.9248	0.9577	72	MelbournePedestrian	0.9573	0.9542	0.9570	<b>0.9652</b>	0.8466	0.9521
7	Beef	<b>0.8667</b>	0.8333	0.8500	0.7500	0.8000	0.8167	73	MiddleAgeGroup.	0.8701	0.8430	<b>0.9134</b>	0.8179	0.7743	0.8304
8	BeetleFly	0.9750	<b>1.0000</b>	0.9800	0.8750	0.8500	0.9250	74	MiddleCorrect.	0.9204	<b>0.9260</b>	0.9150	0.8598	0.8239	0.9070
9	BirdChicken	0.9000	<b>0.9250</b>	0.8750	<b>0.9250</b>	<b>0.9250</b>	0.8500	75	MiddlePhalanxTW	0.8376	0.8179	<b>0.8629</b>	0.7203	0.6746	0.8305
10	BME	0.9944	<b>1.0000</b>	0.9944	0.9944	<b>1.0000</b>	0.9944	76	MixedRegular.	<b>0.9757</b>	0.9750	0.9713	0.9627	0.9350	0.9682
11	Car	<b>0.9583</b>	0.9167	0.9483	0.9250	0.9333	0.9250	77	MixedSmall.	<b>0.9743</b>	0.9695	0.9719	0.9671	0.9446	0.9695
12	CBF	<b>1.0000</b>	<b>1.0000</b>	0.9989	<b>1.0000</b>	0.9978	0.9989	78	MoteStrain	0.9843	0.9843	0.9714	0.9835	0.9764	<b>0.9851</b>
13	Chinatown	0.9890	0.9890	0.9808	<b>0.9896</b>	0.9808	0.9863	79	NonInvasive1.	0.9724	0.9676	<b>0.9787</b>	0.9625	0.9554	0.9625
14	ChlorineCon.	0.9988	0.9988	0.9991	0.9991	0.9025	<b>0.9998</b>	80	NonInvasive2.	<b>0.9782</b>	0.9665	0.9684	0.9636	0.9575	0.9604
15	CinCECGTorso	<b>1.0000</b>	<b>1.0000</b>	0.9993	0.9993	<b>1.0000</b>	0.9993	81	OliveOil	0.8333	0.8167	0.8333	0.8167	0.7333	<b>0.8667</b>
16	Coffee	<b>1.0000</b>	<b>1.0000</b>	<b>1.0000</b>	<b>1.0000</b>	<b>1.0000</b>	<b>1.0000</b>	82	OSULeaf	<b>0.9504</b>	0.9257	0.9302	0.8626	0.8310	0.9077
17	Computers	0.8160	0.8120	0.8040	0.8540	<b>0.8640</b>	0.8240	83	PhalangesOutlines.	0.9300	<b>0.9312</b>	0.9135	0.9022	0.7957	0.9105
18	CricketX	0.9321	0.9064	0.9223	0.9038	0.8538	<b>0.9346</b>	84	Phoneme	<b>0.7844</b>	0.6545	0.6456	0.6234	0.6051	0.6567
19	CricketY	0.9154	0.8808	0.9069	0.8667	0.7974	<b>0.9256</b>	85	PickupGesture.	<b>0.9000</b>	0.8600	0.8900	<b>0.9000</b>	0.8100	0.8200
20	CricketZ	0.9372	0.9013	0.9133	0.8923	0.8179	<b>0.9467</b>	86	PigAirwayPressure	<b>0.6432</b>	0.2446	0.5664	0.5625	0.5662	0.4963
21	Crop	0.8765	0.7342	0.7435	0.7236	0.5973	<b>0.8856</b>	87	PigArtPressure	<b>0.9937</b>	0.8622	0.9904	0.8120	0.6972	0.9745
22	DiatomSizeRe.	<b>1.0000</b>	<b>1.0000</b>	0.9938	0.9938	<b>1.0000</b>	0.9938	88	PigCVP	<b>0.9458</b>	0.7926	0.9172	0.6783	0.6880	0.8344
23	DistalPhalanxOut.	<b>0.9518</b>	0.9462	0.9407	0.8975	0.8961	0.9462	89	PLAID	<b>0.6192</b>	0.5922	0.6025	0.5457	0.4879	0.5383
24	DistalPhalanxOut.	0.9054	<b>0.9077</b>	0.8848	0.8937	0.8631	0.8871	90	Plane	<b>1.0000</b>	0.9952	0.9902	<b>1.0000</b>	0.9952	0.9952
25	DistalPhalanxTW	0.9037	0.9092	0.9203	0.8851	0.8628	<b>0.9292</b>	91	PowerCons	0.9944	0.9917	0.9902	<b>0.9972</b>	0.9806	0.9750
26	DodgerLoopDay	0.8623	0.8625	0.8500	<b>0.8698</b>	0.8183	0.8433	92	ProximalAgeGroup.	0.9091	<b>0.9107</b>	0.9022	0.8810	0.8744	0.9074
27	DodgerLoopGame	<b>0.9433</b>	0.9308	0.9260	0.8813	0.8556	0.9268	93	ProximalCorrect.	0.9294	<b>0.9541</b>	0.9473	0.8485	0.8351	0.9294
28	DodgerLoopWeek.	<b>1.0000</b>	<b>1.0000</b>	0.9917	0.9937	0.9310	0.9935	94	ProximalPhalanxTW	<b>0.9273</b>	0.8876	0.9207	0.8529	0.8612	0.8942
29	Earthquakes	0.8917	0.9135	0.8940	<b>0.9331</b>	0.9135	0.9070	95	RefrigerationDevices	<b>0.8027</b>	0.7347	0.7940	0.7653	0.7480	0.7720
30	ECG200	0.9475	0.9400	0.9400	<b>0.9600</b>	0.9450	0.9050	96	Rock	0.8286	0.8571	<b>0.8857</b>	0.8714	0.8571	0.8286
31	ECG5000	0.9796	0.9810	<b>0.9818</b>	0.9720	0.9566	0.9796	97	ScreenType	0.7027	0.7693	0.7760	<b>0.8253</b>	0.7853	0.6933
32	ECGFiveDays	<b>1.0000</b>	<b>1.0000</b>	<b>1.0000</b>	<b>1.0000</b>	<b>1.0000</b>	<b>1.0000</b>	98	SemgHandGenderCh2	0.9778	0.9211	0.9478	<b>0.9811</b>	0.9211	0.9456
33	ElectricDevices	<b>0.9208</b>	0.8675	0.8756	0.8651	0.7428	0.8654	99	SemgMovementCh2.	0.8256	0.7867	<b>0.8489</b>	0.8300	0.8022	0.8156
34	EOGHorizontalS.	<b>0.9007</b>	0.8386	0.8731	0.8109	0.7612	0.8275	100	SemgHandSubjectCh2	0.9633	<b>0.9667</b>	0.9433	0.9611	0.9489	0.9544
35	EOGVerticalS.	<b>0.8814</b>	0.8413	0.8565	0.7212	0.7861	0.7723	101	ShakeWiimoteZ.	<b>0.9800</b>	0.9600	0.9700	0.9700	0.9100	<b>0.9800</b>
36	EthanolLevel	0.9204	<b>0.9243</b>	0.8895	0.6993	0.7730	0.8446	102	ShapeletSim	0.9950	<b>1.0000</b>	<b>1.0000</b>	0.9350	0.8900	<b>1.0000</b>
37	FaceAll	0.9978	<b>0.9982</b>	0.9908	0.9911	0.9538	0.9973	103	ShapesAll	<b>0.9575</b>	0.9158	0.9508	0.9317	0.8700	0.9442
38	FaceFour	0.9909	<b>1.0000</b>	<b>1.0000</b>	0.9913	0.9913	0.9913	104	SmallAppliances.	0.9053	0.8973	<b>0.9067</b>	0.8813	0.7747	0.8773
39	FacesUCR	0.9956	0.9960	<b>0.9969</b>	0.9880	0.9507	0.9964	105	SmoothSubspace	<b>0.9867</b>	0.9633	0.9800	<b>0.9867</b>	0.9300	0.9800
40	FiftyWords	0.9359	0.8972	<b>0.9414</b>	0.9395	0.8641	0.9359	106	SonyAISurface1.	0.9936	0.9920	0.9936	<b>0.9968</b>	0.9852	0.9936
41	Fish	0.9771	<b>0.9800</b>	<b>0.9800</b>	0.9314	0.9371	0.9571	107	SonyAISurface2.	<b>0.9980</b>	0.9839	0.9909	0.9939	0.9847	0.9969
42	FordA	0.9772	0.9742	<b>0.9811</b>	0.9259	0.8417	0.9793	108	StarLightCurves	<b>0.9905</b>	0.9675	0.9679	0.9563	<b>0.9905</b>	0.9656
43	FordB	<b>0.9744</b>	0.9683	0.9721	0.9240	0.8655	0.9696	109	Strawberry	<b>0.9868</b>	0.9718	0.9756	0.9746	0.9705	0.9827
44	FreezerRegular.	0.9990	0.9990	<b>0.9997</b>	0.9973	0.9877	0.9990	110	SwedishLeaf	<b>0.9867</b>	0.9813	0.9804	0.9778	0.9484	0.9858
45	FreezerSmall.	0.9990	0.9993	<b>0.9997</b>	0.9972	0.9920	0.9986	111	Symbols	<b>0.9941</b>	0.9912	0.9922	0.9863	0.9902	0.9931
46	Fungi	<b>1.0000</b>	<b>1.0000</b>	<b>1.0000</b>	<b>1.0000</b>	0.9951	<b>1.0000</b>	112	SyntheticControl	0.9967	0.9917	0.9905	<b>0.9983</b>	0.9867	0.9917
47	GestureMidAirD1	<b>0.8640</b>	0.7550	0.8553	0.8287	0.8169	0.8201	113	ToeSegmentation1	0.9852	0.9739	<b>0.9855</b>	0.9000	0.9037	0.9741
48	GestureMidAirD2	<b>0.7962</b>	0.6693	0.7847	0.7520	0.6871	0.7584	114	ToeSegmentation2	0.9882	0.9824	<b>0.9884</b>	0.9865	0.9283	0.9820
49	GestureMidAirD3	<b>0.7613</b>	0.5629	0.7226	0.6935	0.6135	0.6815	115	Trace	<b>1.0000</b>	0.9950	0.9950	0.9950	0.9800	<b>1.0000</b>
50	GesturePebbleZ1	0.9867	0.9934	<b>0.9967</b>	0.9672	0.9606	<b>0.9967</b>	116	TwoLeadECG	<b>1.0000</b>	0.9991	0.9981	0.9991	0.9957	0.9991
51	GesturePebbleZ2	<b>0.9836</b>	0.9770	<b>0.9836</b>	0.9738	0.9705	0.9738	117	TwoPatterns	<b>1.0000</b>	<b>1.0000</b>	<b>1.0000</b>	0.9964	0.9864	<b>1.0000</b>
52	GunPoint	0.9900	0.9950	<b>1.0000</b>	0.9900	0.9950	0.9850	118	UMD	0.9944	<b>1.0000</b>	0.9833	0.9889	0.9444	0.9889
53	GunPointAgeSpan	<b>0.9868</b>	0.9867	0.9667	0.9823	0.9801	0.9779	119	UWaveGestureAll.	0.9900	0.9891	0.9931	0.9864	0.9779	<b>0.9933</b>
54	GunPointMale.	0.9956	0.9934	<b>0.9978</b>	0.9956	<b>0.9978</b>	0.9956	120	UWaveGestureX.	<b>0.9406</b>	0.9270	0.9404	0.9087	0.8336	0.9241
55	GunPointOld.	0.9779	0.9778	0.9845	0.9712	0.9601	<b>0.9889</b>	121	UWaveGestureY.	<b>0.9109</b>	0.9044	0.9013	0.8881	0.7224	0.9087
56	Ham	0.9161	0.9116	<b>0.9395</b>	0.9349	0.9301	0.8882	122	UWaveGestureZ.	<b>0.9170</b>	0.8706	0.8704	0.8591	0.7722	0.8841
57	HandOutlines	<b>0.9533</b>	0.9365	0.9000	0.9343	0.9197	0.9248	123	Wafer	<b>1.0000</b>	0.9999	0.9996	0.9996	0.9990	<b>1.0000</b>
58	Haptics	0.7522	0.6770	<b>0.7652</b>	0.7349	0.7327	0.6744	124	Wine	<b>0.8842</b>	0.7763	0.7225	0.6036	0.5047	0.8115
59	Herring	0.7671	0.7351	0.7985	0.7828	<b>0.8375</b>	0.7991	125	WordSynonyms	<b>0.9175</b>	0.8961	0.9093	0.8873	0.8331	0.9094
60	HouseTwenty	0.9688	<b>0.9750</b>	0.9550	0.9698	0.9375	0.9688	126	Worms	0.8453	0.8304	0.8305	0.8458	<b>0.8583</b>	0.7834
61	InlineSkate	<b>0.8077</b>	0.6908	0.7169	0.7246	0.7062	0.7431	127	WormsTwoClass	<b>0.8802</b>	0.8786	0.8648	0.8307	0.8380	0.8726
62	InsectEPGR.	0.9968	<b>1.0000</b>	0.9968	0.9329	0.9744	0.9936	128	Yoga	<b>0.9830</b>	0.9788	0.9773	0.9703	0.9230	0.9609

samples, length 166) and *HouseTwenty* (159 samples, length 2,000) datasets. It is important to note that MR-H is executed on a CPU because its core modules do not use deep learning techniques, whereas other deep learning methods are run on an NVIDIA GeForce RTX 3090 GPU. As shown in Table 14, the differences in inference time between the deep learning methods are negligible. However, we observed that SoftShape demonstrates a slight advantage in inference time on the *HouseTwenty* dataset, which has a longer sequence length.

Table 12: The detailed test classification accuracy of sparse ratios on 18 UCR datasets. The best results are in **bold**.

Dataset	$1 - \eta = 0$	$1 - \eta = 0.1$	$1 - \eta = 0.3$	$1 - \eta = 0.5$	$1 - \eta = 0.7$	$1 - \eta = 0.9$
ArrowHead	0.9576	0.9576	0.9576	0.9435	<b>0.9717</b>	0.9435
CBF	<b>1.0000</b>	<b>1.0000</b>	<b>1.0000</b>	<b>1.0000</b>	<b>1.0000</b>	<b>1.0000</b>
CricketX	0.9365	<b>0.9375</b>	0.9331	0.9321	0.9211	0.9006
DistalPhalanxOutlineAgeGroup	0.9529	0.9510	0.9288	0.9518	<b>0.9530</b>	0.8861
DistalPhalanxOutlineCorrect	0.8951	0.8871	<b>0.9055</b>	0.9054	0.8780	0.8734
ECG5000	0.9772	0.9802	<b>0.9810</b>	0.9796	<b>0.9810</b>	0.9696
EOGVerticalSignal	0.9145	<b>0.9321</b>	0.9310	0.9007	0.8730	0.8690
EthanolLevel	<b>0.9214</b>	0.9205	0.9205	0.9204	0.8985	0.8856
Fish	0.9742	<b>0.9799</b>	0.9656	0.9771	0.9628	0.9713
GunPoint	0.9850	0.9750	0.9850	<b>0.9900</b>	0.9850	0.9850
InsectWingbeatSound	0.8828	0.8760	0.8819	<b>0.8882</b>	0.8700	0.8860
ItalyPowerDemand	0.9891	<b>0.9917</b>	0.9846	0.9891	0.9837	0.9901
MelbournePedestrian	0.9511	<b>0.9603</b>	0.9545	0.9573	0.9391	0.9319
MiddlePhalanxTW	0.8340	0.8322	0.8268	<b>0.8376</b>	0.7474	0.7781
MixedShapesRegularTrain	0.9784	0.9781	<b>0.9801</b>	0.9757	0.9644	0.9620
OSULeaf	0.9414	0.9491	0.9413	<b>0.9504</b>	0.9436	0.9256
Trace	<b>1.0000</b>	<b>1.0000</b>	<b>1.0000</b>	<b>1.0000</b>	<b>1.0000</b>	<b>1.0000</b>
WordSynonyms	<b>0.9382</b>	0.9360	0.9294	0.9161	0.9095	0.9128
Avg. Acc	0.9461	<b>0.9469</b>	0.9448	0.9453	0.9323	0.9261
Avg. Rank	2.44	<b>2.39</b>	2.78	2.61	3.89	4.50
Win	4	<b>7</b>	5	6	5	2

#### B.4. Hyperparameter Analysis

Table 15 provides the test classification accuracy results of SoftShape on 18 UCR time series datasets when varying the sliding fixed step size ( $q$ ). Table 16 presents the detailed test classification accuracy results of SoftShape across 18 UCR time series datasets for different model depth ( $L$ ) values. Table 17 presents the detailed test classification accuracies of SoftShape across 18 UCR datasets, evaluated with varying setting shape lengths  $m$ .

Tables 18, 19, 20, and 21 present the statistical test classification results of SoftShape on 18 selected UCR time series datasets. The evaluations are conducted under varying conditions, including different maximum numbers of experts for intra-shape learning, class-specific MoE expert networks, shared expert networks, and hyperparameter  $\lambda$ . For clarity and ease of analysis, only the statistical results of test accuracies are reported in Tables 18, 19, 20, and 21.

#### B.5. Time Series Forecasting Results

For the forecasting task, we evaluate SoftShape on the *ETTh1*, *ETTh2*, *ETTm1*, and *ETTm2* datasets, using TS2Vec (Yue et al., 2022), TimesNet (Wu et al., 2023a), PatchTST (Nie et al., 2023), GPT4TS (Zhou et al., 2023), and iTransformer (Liu et al., 2024b) as baselines. Following the experimental setup of (Ma et al., 2024), we report the Mean Squared Error (MSE) and Mean Absolute Error (MAE) for all methods in Tables 22 and 23. Notably, we do not adjust hyperparameters for SoftShape across the four datasets, nor do we modify its shape embedding layer as done in (Nie et al., 2023). The results demonstrate that SoftShape outperforms TS2Vec and TimesNet, highlighting its potential for time series forecasting tasks.

Table 13: The detailed test accuracy of the number of activated experts on 18 UCR datasets. The best results are in **bold**.

Dataset	$k=1$	$k=2$	$k=3$	$k=4$
ArrowHead	<b>0.9435</b>	0.9324	0.9196	0.9147
CBF	<b>1.0000</b>	<b>1.0000</b>	<b>1.0000</b>	<b>1.0000</b>
CricketX	0.9321	<b>0.9487</b>	0.9334	0.9475
DistalPhalanxOutlineAgeGroup	0.9518	<b>0.9665</b>	0.9221	0.9518
DistalPhalanxOutlineCorrect	<b>0.9054</b>	0.8517	0.8574	0.8517
ECG5000	0.9796	<b>0.9840</b>	0.9792	0.9640
EOGVerticalSignal	0.9007	0.9381	<b>0.9490</b>	0.9353
EthanolLevel	0.9204	<b>0.9264</b>	0.9054	0.9164
Fish	<b>0.9771</b>	0.9513	0.9571	0.9656
GunPoint	<b>0.9900</b>	0.9850	0.9850	0.9850
InsectWingbeatSound	<b>0.8882</b>	0.8782	0.8732	0.8659
ItalyPowerDemand	<b>0.9891</b>	0.9809	0.9809	0.9873
MelbournePedestrian	0.9573	0.9581	0.9568	<b>0.9601</b>
MiddlePhalanxTW	0.8376	0.8429	0.8231	<b>0.8719</b>
MixedShapesRegularTrain	<b>0.9757</b>	0.9675	0.8629	0.9535
OSULeaf	<b>0.9504</b>	0.9302	0.9390	0.8963
Trace	<b>1.0000</b>	<b>1.0000</b>	<b>1.0000</b>	<b>1.0000</b>
WordSynonyms	0.9161	0.9580	0.9536	<b>0.9625</b>
<b>Avg. Acc</b>	<b>0.9453</b>	0.9444	0.9332	0.9405
<b>Avg. Rank</b>	<b>1.89</b>	1.94	2.78	2.39
<b>Win</b>	<b>10</b>	6	3	5

Table 14: Comparison of model parameter counts and inference times.

Methods	# Parameters	# Inference Time (Seconds)	
		ChlorineConcentration	HouseTwenty
MR-H	-	6.60	2.97
InceptionTime	387.7 K	1.41	1.30
TSLANet	514.6 K	<b>1.37</b>	1.29
Medformer	1360.6 K	1.48	1.31
<b>SoftShape (Ours)</b>	472.5 K	1.39	<b>1.26</b>



Table 15: The detailed test classification accuracy of sliding step size  $q$  on 18 UCR datasets. The best results are in **bold**.

Dataset	$q=1$	$q=2$	$q=3$	$q=4$	$q=m$
ArrowHead	0.8913	0.9289	0.9431	0.9435	<b>0.9451</b>
CBF	<b>1.0000</b>	<b>1.0000</b>	<b>1.0000</b>	<b>1.0000</b>	<b>1.0000</b>
CricketX	0.8936	0.9231	0.9103	<b>0.9321</b>	0.9295
DistalPhalanxOutlineAgeGroup	0.9147	<b>0.9629</b>	0.9610	0.9518	0.9184
DistalPhalanxOutlineCorrect	0.8688	0.8837	0.8540	<b>0.9054</b>	0.8632
ECG5000	0.9672	0.9734	0.9822	0.9796	<b>0.9824</b>
EOGVerticalSignal	0.8551	0.9104	0.9408	0.9007	<b>0.9533</b>
EthanolLevel	0.8656	0.8736	<b>0.9294</b>	0.9204	0.8786
Fish	0.9485	0.9513	0.9713	<b>0.9771</b>	0.9399
GunPoint	0.9800	0.9850	0.9650	<b>0.9900</b>	0.9800
InsectWingbeatSound	0.7922	0.8563	0.8582	<b>0.8882</b>	0.8741
ItalyPowerDemand	0.9818	0.9873	<b>0.9918</b>	0.9891	0.9891
MelbournePedestrian	0.9538	0.9480	0.9518	<b>0.9573</b>	0.9431
MiddlePhalanxTW	0.7451	0.8267	<b>0.8629</b>	0.8376	0.7724
MixedShapesRegularTrain	0.9477	0.9272	0.8783	<b>0.9757</b>	0.9157
OSULeaf	0.9300	<b>0.9774</b>	0.9525	0.9504	0.9204
Trace	<b>1.0000</b>	<b>1.0000</b>	<b>1.0000</b>	<b>1.0000</b>	<b>1.0000</b>
WordSynonyms	0.8310	0.9017	<b>0.9172</b>	0.9161	0.8261
<b>Avg. Acc</b>	0.9092	0.9343	0.9372	<b>0.9453</b>	0.9240
<b>Avg. Rank</b>	3.83	2.78	2.44	<b>1.78</b>	2.94
<b>Win</b>	2	4	5	<b>9</b>	5

Table 16: The detailed test classification accuracy of model depth  $L$  on 18 UCR datasets. The best results are in **bold**.

Dataset	$L=1$	$L=2$	$L=3$	$L=4$	$L=5$	$L=6$
ArrowHead	<b>0.9437</b>	0.9435	0.9390	0.9155	0.9155	0.9251
CBF	<b>1.0000</b>	<b>1.0000</b>	0.9989	0.9978	0.9989	0.9989
CricketX	0.8962	0.9321	0.9706	<b>0.9783</b>	0.9501	0.9539
DistalPhalanxOutlineAgeGroup	0.9629	0.9518	0.9740	0.9389	<b>0.9741</b>	0.9574
DistalPhalanxOutlineCorrect	0.9054	0.9054	0.8917	0.8962	0.8811	<b>0.9077</b>
ECG5000	<b>0.9830</b>	0.9796	0.9770	0.9750	0.9810	0.9790
EOGVerticalSignal	0.8038	0.9007	0.9187	<b>0.9422</b>	0.9083	0.8979
EthanolLevel	0.8189	<b>0.9204</b>	0.8905	0.8975	0.9005	0.8945
Fish	0.9428	0.9771	0.9914	0.9914	0.9685	<b>0.9942</b>
GunPoint	0.9800	<b>0.9900</b>	<b>0.9900</b>	<b>0.9900</b>	<b>0.9900</b>	<b>0.9900</b>
InsectWingbeatSound	<b>0.9237</b>	0.8882	0.8905	0.8968	0.8764	0.8777
ItalyPowerDemand	0.9854	0.9891	<b>0.9982</b>	0.9864	0.9937	0.9882
MelbournePedestrian	<b>0.9589</b>	0.9573	0.9488	0.9567	0.9531	0.9578
MiddlePhalanxTW	0.8070	<b>0.8376</b>	0.7799	0.8052	0.7979	0.8124
MixedShapesRegularTrain	0.9282	0.9757	0.9778	<b>0.9781</b>	0.9689	0.9747
OSULeaf	0.9368	0.9504	0.9503	0.9414	<b>0.9571</b>	0.9233
Trace	<b>1.0000</b>	<b>1.0000</b>	<b>1.0000</b>	<b>1.0000</b>	<b>1.0000</b>	<b>1.0000</b>
WordSynonyms	0.8344	0.9161	0.9062	0.8974	0.8951	<b>0.9228</b>
<b>Avg. Acc</b>	0.9228	<b>0.9453</b>	0.9441	0.9436	0.9395	0.9420
<b>Avg. Rank</b>	3.72	<b>2.61</b>	3.06	3.33	3.44	3.06
<b>Win</b>	<b>6</b>	5	3	5	4	4

Table 17: The detailed test classification accuracy of shape length  $m$  on 18 UCR datasets. The best results are in **bold**.

Dataset	Val-Select	Fixed-8	Multi-Seq
ArrowHead	0.9435	0.9435	<b>0.9436</b>
CBF	<b>1.0000</b>	<b>1.0000</b>	<b>1.0000</b>
CricketX	<b>0.9321</b>	0.9282	0.9320
DistalPhalanxOutlineAgeGroup	0.9518	<b>0.9611</b>	0.9351
DistalPhalanxOutlineCorrect	0.9054	0.9065	<b>0.9156</b>
ECG5000	0.9796	0.9610	<b>0.9810</b>
EOGVerticalSignal	<b>0.9007</b>	0.8759	0.8952
EthanolLevel	0.9204	0.8785	<b>0.9303</b>
Fish	<b>0.9771</b>	0.9686	0.9697
GunPoint	<b>0.9900</b>	<b>0.9900</b>	<b>0.9900</b>
InsectWingbeatSound	0.8882	0.9010	<b>0.9055</b>
ItalyPowerDemand	<b>0.9891</b>	0.9855	0.9867
MelbournePedestrian	0.9573	0.9641	<b>0.9647</b>
MiddlePhalanxTW	0.8376	0.8352	<b>0.8414</b>
MixedShapesRegularTrain	0.9757	0.9808	<b>0.9849</b>
OSULeaf	<b>0.9504</b>	0.9392	0.9444
Trace	<b>1.0000</b>	<b>1.0000</b>	<b>1.0000</b>
WordSynonyms	<b>0.9161</b>	0.9028	0.9139
<b>Avg. Acc</b>	0.9453	0.9401	<b>0.9463</b>
<b>Avg. Rank</b>	1.72	2.28	<b>1.44</b>
<b>Win</b>	9	4	<b>11</b>

 Table 18: The statistical test classification accuracy of the total number of experts  $\hat{C}$  on 18 UCR datasets. And  $C$  denotes the total number of classes within each time series dataset. The best results are in **bold**.

Metric	$\hat{C}=C/2$	$\hat{C}=C$	$\hat{C}=2C$
Avg. Acc	0.9215	<b>0.9453</b>	0.9408
Avg. Rank	2.33	<b>1.39</b>	1.83
Win	4	<b>12</b>	6

 Table 19: The statistical test classification accuracy across different networks used as MoE experts on 18 UCR datasets. TSLANet (ICB) indicates that the ICB block within TSLANet is used as the MoE expert. The best results are in **bold**.

Metric	FCN	TSLANet (ICB)	Original MoE expert
Avg. Acc	0.8652	0.9049	<b>0.9453</b>
Avg. Rank	2.56	1.83	<b>1.44</b>
Win	4	7	<b>10</b>

 Table 20: The statistical test classification accuracy and parameter counts across different networks used as the shared expert on 18 UCR datasets. The best results are in **bold**.

Metric	Transformer	MLP	Inception
# Parameters	422.5 K	157.8 K	179.5 K
Avg. Acc	0.8239	0.8103	<b>0.9453</b>
Avg. Rank	2.22	2.44	<b>1.11</b>
Win	4	1	<b>16</b>

Table 21: The statistical test classification accuracy across different  $\lambda$  on 18 UCR datasets. The best results are in **bold**.

Metric	$\lambda = 0.0001$	$\lambda = 0.001$	$\lambda = 0.01$	$\lambda = 0.1$	$\lambda = 1$	$\lambda = 10$	$\lambda = 100$
Avg. Acc	0.9417	0.9453	<b>0.9471</b>	0.9374	0.9394	0.9438	0.9431
Avg. Rank	3.00	<b>2.50</b>	2.61	4.11	3.72	3.72	3.56
Win	6	6	<b>8</b>	4	4	5	7

 Table 22: The detailed test forecasting performance (Mean Squared Error, MSE) of different methods. The best results are in **bold**.

Methods		TS2Vec	TimesNet	PatchTST	GPT4TS	iTransformer	<b>SoftShape (Ours)</b>
Metric		MSE	MSE	MSE	MSE	MSE	MSE
ETTh1	24	0.5952	0.3485	0.3890	0.3102	<b>0.3065</b>	0.5239
	48	0.6316	0.3991	0.4362	0.3529	<b>0.3451</b>	0.5160
	168	0.7669	0.4846	0.5304	0.4600	<b>0.4307</b>	0.4564
	336	0.9419	0.5583	0.5928	0.5167	<b>0.4889</b>	0.4992
	720	1.0948	0.5886	0.6123	0.6878	0.5184	0.5099
	Avg. Value	0.8061	0.4758	0.5121	0.4655	<b>0.4179</b>	0.5011
	Avg. Rank	6	3.4	4.4	3	<b>1.2</b>	3
ETTh2	24	0.4478	0.2129	0.2176	0.2009	<b>0.1831</b>	0.2542
	48	0.6460	0.2824	0.2722	0.2738	<b>0.2413</b>	0.2808
	168	1.7771	0.4461	0.4092	0.4436	<b>0.3725</b>	0.3824
	336	2.1157	0.4875	0.4670	0.5011	<b>0.4368</b>	0.4429
	720	2.5823	0.5193	0.4721	0.5389	<b>0.4479</b>	0.4722
	Avg. Value	1.5138	0.3896	0.3676	0.3917	<b>0.3363</b>	0.3665
	Avg. Rank	6	4.2	2.8	3.8	<b>1</b>	3.2
ETTm1	24	0.1970	0.2416	0.2522	0.2004	0.2251	0.2980
	48	0.2682	0.3194	0.3202	0.3006	0.3019	0.3197
	96	0.3735	0.3558	0.3553	0.3008	0.3393	0.3389
	288	0.7566	0.4411	0.4207	0.3712	0.4147	0.3953
	672	1.8217	0.6567	0.4878	0.4570	0.4880	0.4706
	Avg. Value	0.6834	0.4029	0.3672	<b>0.3260</b>	0.3538	0.3645
	Avg. Rank	4	4.6	4.4	<b>1.4</b>	3.2	3.4
ETTm2	96	0.3502	0.1877	0.1876	0.1861	<b>0.1830</b>	0.1873
	192	0.5684	0.2748	0.2544	0.2624	<b>0.2507</b>	0.2545
	336	0.9589	0.3922	0.3173	<b>0.3164</b>	0.3179	0.3190
	720	2.5705	0.4477	0.4179	0.4246	<b>0.4161</b>	0.4248
	Avg. Value	1.1120	0.3256	0.2943	0.2974	<b>0.2919</b>	0.2964
	Avg. Rank	5.6	4.92	2.88	2.28	<b>1.84</b>	3.48

Table 23: The detailed test forecasting performance (Mean Absolute Error, MAE) of different methods. The best results are in **bold**.

Methods		TS2Vec	TimesNet	PatchTST	GPT4TS	iTransformer	<b>SoftShape (Ours)</b>
Metric		MAE	MAE	MAE	MAE	MAE	MAE
ETTh1	24	0.5313	0.3873	0.4128	0.3626	<b>0.3589</b>	0.4817
	48	0.5566	0.4169	0.4379	0.3904	<b>0.3818</b>	0.4794
	168	0.6405	0.4670	0.4879	0.4661	<b>0.4304</b>	0.4481
	336	0.7334	0.5175	0.5193	0.4960	<b>0.4602</b>	0.4719
	720	0.8098	0.5287	0.5442	0.5858	<b>0.4982</b>	0.4951
	Avg. Value	0.6543	0.4635	0.4804	0.4602	<b>0.4259</b>	0.4752
	Avg. Rank	6	3.4	4.4	3	<b>1.2</b>	3
ETTh2	24	0.5032	0.2929	0.3043	0.2917	<b>0.2719</b>	0.3344
	48	0.6184	0.3429	0.3388	0.3443	<b>0.3120</b>	0.3475
	168	1.0569	0.4361	0.4172	0.4476	<b>0.3940</b>	0.4042
	336	1.1759	0.4687	0.4610	0.4876	<b>0.4433</b>	0.4484
	720	1.3521	0.4893	0.4734	0.5146	<b>0.4585</b>	0.4721
	Avg. Value	0.9413	0.4060	0.3989	0.4172	<b>0.3759</b>	0.4013
	Avg. Rank	6	3.6	3	4.2	<b>1</b>	3.2
ETTm1	24	0.3179	0.3115	0.3186	0.2769	0.2967	0.3564
	48	0.3784	0.3637	0.3593	0.3344	0.3474	0.3644
	96	0.4496	0.3864	0.3793	0.3519	0.3740	0.3751
	288	0.6672	0.4304	0.4162	0.3989	0.4163	0.4072
	672	1.0452	0.5324	0.4527	0.4483	0.4577	0.4512
	Avg. Value	0.5717	0.4049	0.3852	<b>0.3621</b>	0.3784	0.3908
	Avg. Rank	5.6	4.4	3.6	<b>1</b>	2.8	3.6
ETTm2	96	0.4381	0.2678	0.2728	0.2781	<b>0.2652</b>	0.2744
	192	0.5732	0.3220	0.3140	0.3271	<b>0.3101</b>	0.3167
	336	0.7532	0.3830	0.3527	0.3650	<b>0.3524</b>	0.3572
	720	1.2483	0.4244	<b>0.4075</b>	0.4331	0.4090	0.4186
	Avg. Value	0.7532	0.3493	0.3367	0.3508	<b>0.3342</b>	0.3418
	Avg. Rank	5.92	3.88	2.32	4	<b>1.56</b>	3.32